

# SeaQuest with a Transversely Polarized Target (E1039)

M. Brooks, A. Klein (CoSpokesperson), D. Kleinjan, K. Liu, M. Liu  
M. McCumber, P. McGaughey, C. Da Silva  
*Los Alamos National Laboratory, Los Alamos, NM 87545*

J. Arrington, D. Geesaman, M. Mesquita de Medeiros, P. Reimer, Z. Ye  
*Argonne National Laboratory, Argonne, IL 60439*

C. Brown, D. Christian  
*Fermi National Accelerator Laboratory, Batavia IL 60510*

J.-C. Peng  
*University of Illinois, Urbana, IL 61081*

W.-C. Chang, Y.-C. Chen  
*Institute of Physics, Academia Sinica, Taiwan*

S. Sawada  
*KEK, Tsukuba, Ibaraki 305-0801, Japan*

T.-H. Chang  
*Ling-Tung University, Taiwan*

C. Aidala, W. Lorenzon, R. Raymond  
*University of Michigan, Ann Arbor, MI 48109-1040*

T. Badman, E. Long, K. Slifer, R. Zielinski  
*University of New Hampshire, Durham, NH 03824*

R.-S. Guo  
*National Kaohsiung Normal University, Taiwan*

Y. Goto  
*RIKEN, Wako, Saitama 351-01, Japan*

J.-P. Chen  
*Thomas Jefferson National Accelerator Facility, Newport News, VA 23606*

K. Nakano, T.-A. Shibata  
*Tokyo Institute of Technology, Tokyo 152-8551, Japan*

D. Crabb, D. Day, D. Keller (CoSpokesperson), O. Rondon  
*University of Virginia, Charlottesville, VA 22904*

G. Dodge, S. Bueltmann  
*Old Dominion University, Norfolk VA 23936*

J. Dunne, D. Dutta, L. El Fassi,  
*Mississippi State University, Starkville, MS 39762*

E. Kinney  
*University of Colorado, Boulder, CO 80309*

N. Doshita, T. Iwata, Y. Miyachi  
*Yamagata University, Yamagata 990-8560, Japan*

M. Daugherty, D. Isenhower, R. Towell, S. Watson  
*Abilene Christian University, Abilene, TX 79601*

## Abstract

We have constructed a state-of-the-art, high luminosity polarized proton and deuteron target and propose to measure the Sivers asymmetry for the  $\bar{u}$  and  $\bar{d}$  sea quarks in the nucleon for four different Bjorken  $x_B$  bins in the range  $0.1 < x_B < 0.5$ , using the Drell-Yan process at SeaQuest. We will: i) perform the first measurement of the Sivers asymmetry in Drell-Yan scattering for sea quarks; ii) determine the flavor dependence of the Sivers function for the  $\bar{u}$  and  $\bar{d}$  sea quarks iii) explore a unique range of virtualities and transverse momenta not accessible through  $Z^0/W^\pm$  measurements; and iv) determine the sign and possibly the magnitude of the sea quark Sivers function in Drell-Yan for comparison to future sea quark Sivers function determinations in Semi Inclusive Deep Inelastic Scattering (SIDIS). Measuring a nonzero Sivers asymmetry would provide “smoking gun” evidence for nonzero orbital angular momentum of sea quarks; determination of the  $\bar{u}$  and  $\bar{d}$  Sivers function would allow comparison of the sea quark Sivers function flavor dependence to that for valence quarks; and measuring a sign change in the Sivers asymmetry between this measurement and future measurements at the EIC would test a fundamental prediction of QCD.

This proposal seeks funding from DOE Office of Nuclear Physics for the installation of the E-1039 experiment, which could be the beginning of an exciting new spin physics program at Fermilab that is complementary to the spin physics programs at RHIC and JLab.

## Abstract

# Contents

<b>1</b>	<b>Introduction</b>	<b>5</b>
<b>2</b>	<b>Motivation</b>	<b>8</b>
2.1	The Drell Yan Process . . . . .	8
2.2	Theory . . . . .	9
2.2.1	TMDs . . . . .	11
2.2.2	Orbital Angular Momentum . . . . .	14
2.3	Current theoretical and experimental status . . . . .	15
2.4	The angular dependence of the Drell-Yan cross section . . . . .	16
2.5	The Measurements . . . . .	18
2.5.1	$p + p^\uparrow$ . . . . .	18
2.5.2	$p + d^\uparrow$ . . . . .	18
3.2	The Polarized Target . . . . .	20
3.3	Beamline . . . . .	21
3.5	Count Rates and Statistical Errors . . . . .	23
3.4	Integration of the polarized target into SeaQuest . . . . .	23
3.6	Polarization Measurements . . . . .	24
3.6.1	Proton Polarization Measurements . . . . .	24
3.6.2	Neutron Polarization Measurements . . . . .	25
3.6.3	Target Polarization Uncertainty . . . . .	26
3.6.4	Active Target Contributions . . . . .	27
3.7	Luminosity and Beam Intensity Uncertainty . . . . .	27
3.7.1	Beam Profile . . . . .	27
3.7.2	Luminosity measurement . . . . .	27
3.7.3	Consistency in Delivered Luminosity . . . . .	28
3.8	Spectrometer Induced Uncertainties . . . . .	29
3.9	Overall Systematic Error . . . . .	30
3.10	Expected Results . . . . .	30
<b>4</b>	<b>Comparison to Competition</b>	<b>31</b>
<b>5</b>	<b>Budget Discussion</b>	<b>32</b>
5.1	Liquefier System and Pump Installation . . . . .	33
5.2	Beam Line Changes . . . . .	33
5.3	Shielding and Target Cave Modifications . . . . .	33
5.4	Total Installation Costs . . . . .	34
	<b>Appendices</b>	<b>34</b>
<b>A</b>	<b>Fermilab PAC 2013 and 2015 reviews</b>	<b>34</b>

<b>B</b>	<b>The current accomplishments from the LDRD</b>	<b>35</b>
B.1	Experimental . . . . .	35
B.2	Theoretical . . . . .	37
B.3	LANL reviews . . . . .	37
<b>C</b>	<b>Future Physics Opportunities</b>	<b>38</b>
C.1	Deuteron Tensor Function $b_1$ . . . . .	38
C.2	Explore gluon TMD/Twist-3 trigluon correlation functions and QCD dynamics with heavy quarks . . . . .	39
<b>D</b>	<b>Letter of Intent P-1039</b>	<b>41</b>
<b>E</b>	<b>Quote For Liquefier</b>	<b>48</b>

# 1 Introduction

The central challenge of nuclear and particle spin physics is to disentangle exactly how the nucleon's spin is built up from its quark and gluon constituents. It is well known that the proton is a spin-1/2 particle, but how the constituents assemble into this quantized spin is still a mystery. Since the discovery of the "spin crisis" by the EMC collaboration [1], the global physics community, with the support of the Department of Energy Office of Nuclear Physics has embarked on a multidecade program to determine the individual contributions to the proton spin [2] [3]. Experiments have established that the valence quark spins contribute around 30%, while the gluon intrinsic angular momentum is still under active investigation at the Relativistic Heavy Ion Collider [4].

Tremendous progress has been made during the past few decades in measuring the parton distribution functions (PDF), describing the longitudinal momentum distributions of the partons inside a nucleon, as well as measuring the helicity distributions, which sample the amount of partons with longitudinal spin parallel or antiparallel to the spin of the parent nucleon. While these data describe number densities for the partons, they do not provide for the description of the motion of the partons inside the nucleons, since they originate from a collinear configuration, describing only longitudinal degrees of freedom. Considering the following four points

1. The uncertainty principle for a quark confined within a nucleon provides an intrinsic transverse momentum  $k_T \sim 200 \text{ MeV}/c$
2. Collinear gluon emission from a massless quark is forbidden by the helicity conservation of pQCD
3. Neither Semi Inclusive Deep Inelastic Scattering (SIDIS) nor Drell Yan processes are intrinsically collinear at finite  $p_T$ , as can be seen in Figs. 1 and 2
4. Measurements of quark hadronization into jets show them not to be collinear

it becomes natural to include the intrinsic transverse motion of the partons, which is needed to achieve a complete three dimensional description of the nucleon.

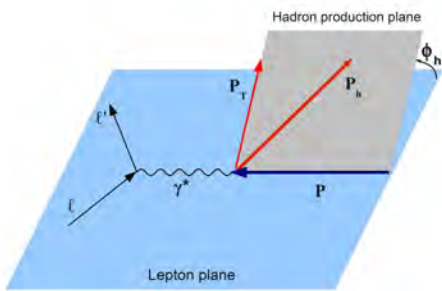


Figure 1: *SIDIS kinematics*

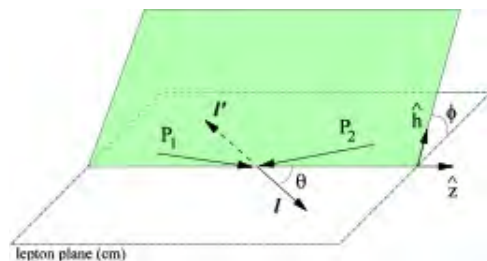


Figure 2: *The Drell Yan process in the Collins-Soper frame*

Studies of hadrons produced in unpolarized SIDIS [5] (see Fig. 3) and hadron production [6] (see Fig. 4) experiments exhibit significant azimuthal asymmetries, which are directly related to the transverse momentum of the partons. To describe this transverse structure, new functions that arise from operators allowed by the symmetries of Quantum Chromodynamics (QCD) are required, the so called Transverse Momentum Distributions (TMD). These TMDs encode the

relation between the transverse spin and the transverse momentum of the partons and nucleons. Among the eight TMDs, the Sivers [7] and the Boer-Mulders [8] functions, both naive T-odd, play a prominent role with both of them being connected to the parton angular momentum. The Sivers function represents the correlation of the transverse momentum of an unpolarized parton with the spin of a transversely polarized nucleon, while the Boer-Mulders function expresses the connection between the transverse parton polarization and its transverse momentum in an unpolarized nucleon. The Sivers function was originally proposed to explain the large transverse

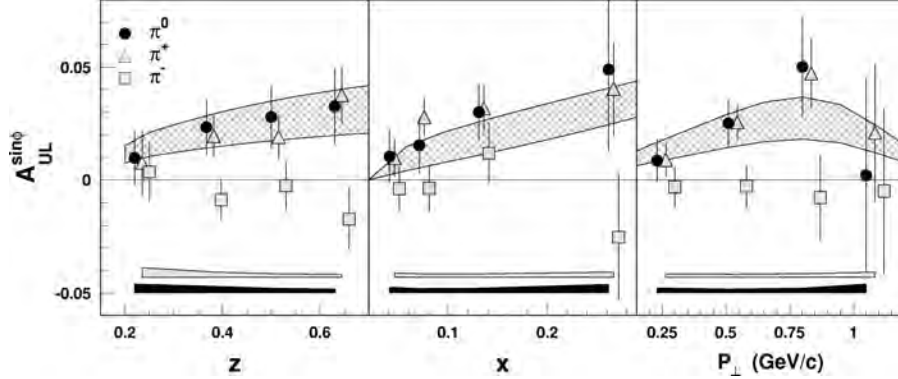


Figure 3: *Analyzing power for pion electro production by HERMES [5]*

single spin asymmetries seen in hadron-hadron scattering experiments dating back to the 1970’s. D. Sivers [7] suggested that the  $k_T$  distribution of the partons could have an azimuthal asymmetry, when the hadron was transversely polarized. Shortly thereafter, E704 [6] published their seminal result on pion production, (see Fig. 4). In addition, a fundamental prediction of QCD is that the Sivers function has to be equal in magnitude and opposite in sign when measured in SIDIS and Drell-Yan [18]. This prediction is deeply rooted in the gauge structure of QCD as a field theory, and is based on the well-known QCD factorization formalism widely used in interpreting high-energy experimental data. Thus, its experimental verification or refutation is crucial. NSAC milestone HP13 was therefore established to “test unique QCD predictions for relations between single transverse spin phenomena in p-p scattering and those observed in deep inelastic lepton scattering.”

HERMES [12], COMPASS [13] and Jlab [14] have measured non zero values of the Sivers function of the nucleon, with the data indicating that the **valence** d-quark and u-quark Sivers functions are approximately equal and opposite in sign. However, data for sea quarks are notably lacking. While SIDIS only permits the measurement of a convolution of the Sivers function with a fragmentation function, Drell-Yan allows the direct measurement of the Sivers function without the complications of fragmentation functions and final state interactions. Coupled with its innate sensitivity to sea quarks, Drell-Yan is therefore a clean probe to determine the Sivers function for the sea quarks.

We propose to carry out the first measurement of the sea quark Sivers function, using Drell-Yan production from an unpolarized 120 GeV proton beam interacting with transversely polarized proton and neutron targets. This experiment has obtained stage one approval by Fermilab management as experiment E1039. With this proposal, we are seeking the funding that will allow the execution of the experiment. Using the antiquark selectivity of Drell-Yan, we will make the first ever determination of the size and the sign of the sea quark  $\bar{u}(x)$  Sivers function with our results also allowing a test of the fundamental prediction of QCD.

Since our target system will contain polarized  $\text{NH}_3$  (the proton target) and polarized  $\text{ND}_3$  (as

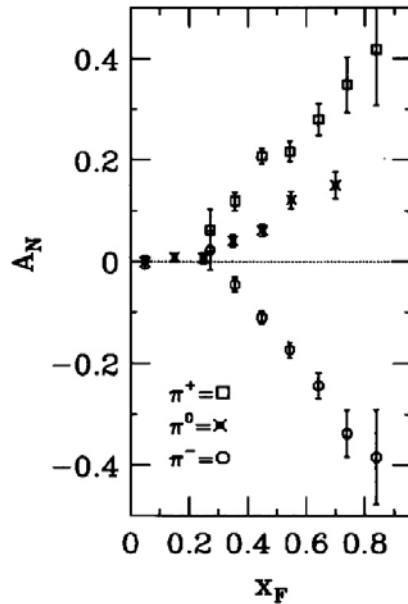


Figure 4: *Asymmetry in  $pp^\dagger \rightarrow \pi X$  pion production from E704 [6]*

the neutron target) we will be able to determine independently both the  $\bar{u}$  and  $\bar{d}$  contributions; something no other proposed experiment is able to do. We will further be able to determine if there is a flavor asymmetry in the Siverson function of the sea, as has been observed for the valence quarks. Measurements by the NMC collaboration at CERN and the LANL-led Experiment E866 at FNAL showed that the Gottfried Sum Rule, which predicted a symmetric sea quark momentum distribution, was strongly violated (see Fig. 5), indicating that these sea quarks are not only perturbatively generated by gluon splitting.

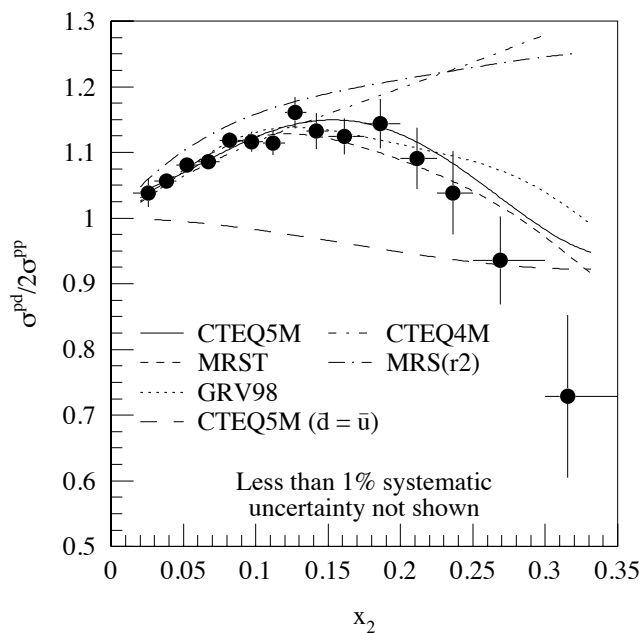


Figure 5: *The Drell-Yan cross section ratio for deuterium versus hydrogen from E866 [10]. The dashed line shows the ratio for a symmetric sea  $\bar{u}(x) = \bar{d}(x)$*

The origin of this violation of perturbative QCD is still not understood and has led to the development of many different theoretical models. Among those, the pion cloud model of the proton, predicts a direct connection between the  $\bar{d}$  excess seen in E866 (see Fig.5) and the orbital angular momentum of the sea.

In summary, E1039 will measure the Sivers asymmetry for both the  $\bar{u}$  and  $\bar{d}$  quarks, within the range of  $0.1 < x_B < 0.5$ . Proton induced Drell-Yan production on polarized proton and deuteron targets has never been performed. These measurements are complementary to the (stage-1) approved experiment E1027 at Fermilab [19], which will measure the Sivers function of the valence quarks using a polarized proton beam on an unpolarized proton target. If the measured sea quark Sivers function is non-zero, we will also determine its sign. While it is clear that the existence of the Sivers function requires non-zero quark orbital angular momentum (OAM), there is no model-independent connection between the Sivers distribution and the size of the quark OAM as of yet, so additional theoretical work is needed to provide a direct connection.

It is important to note that the proposed measurement is the only currently planned experiment which will cleanly access the sea quark Sivers function in a unique virtuality  $Q^2 \sim 10 \text{ GeV}^2$  and transverse momentum  $q_T$  in the few GeV region. Current SIDIS measurements are dominated by the valence quarks and are insensitive to sea quark contributions. The COMPASS experiment at CERN, using pion induced Drell-Yan, probes the valence region due to the antiquark content of the beam. Measurements of single spin asymmetries in  $W^\pm/Z^0$  production at RHIC probe a combination of the Sivers function and the parity-violating transverse helicity distribution  $g_{1T}$  [9]. The virtuality  $Q^2 \sim 10000 \text{ GeV}^2$  and transverse momentum  $q_T \sim 10 \text{ GeV}$  are also vastly different. Such large transverse momenta may also require a nonperturbative theoretical treatment.

While E1039 is a continuation of the SeaQuest experiment, there are some important changes and additions necessary to the current configuration. The installation of the polarized target will require not only some modifications to the beamline to protect the superconducting coils, but also changes to the shielding around the target area and the first magnet. In addition, we will need to purchase a closed loop liquid Helium system, to conform with new DOE requirements on nonrenewable resources. A detailed discussion of these changes can be found in Section 5. In order to cover these initial installation expenses we are asking for support from the DOE Office of Nuclear Physics.

## 2 Motivation

### 2.1 The Drell Yan Process

The Drell-Yan process [20] describes the hadron-hadron collisions, where at tree level a quark from one particle annihilates with an antiquark from the other particle, creating a virtual photon. The virtual photon subsequently decays into two leptons,  $\ell^+$  and  $\ell^-$ . This process is schematically shown in the Feynman diagram in Fig. 6. The Drell-Yan process is one of the cornerstone perturbative QCD processes that cleanly probes the internal structure of the colliding hadrons, has low background, and is free of the fragmentation uncertainties.

In our proposed experiment we will use  $p+ p^\uparrow$  and  $p+ d^\uparrow$ , while COMPASS uses  $\pi+ p^\uparrow$ . To lowest order, the cross section for the Drell Yan process depends on the product of the quark and antiquark distributions  $q, \bar{q}$  in the beam  $x_1$  and in the target  $x_2$ , where  $x_1, x_2$  are the Bjorken  $x$

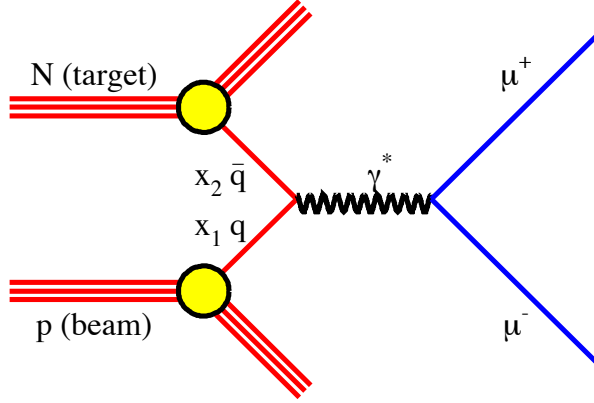


Figure 6: *The Drell-Yan process*

and express the fraction of the longitudinal momentum of the nucleon carried by the quark.

$$\frac{d\sigma}{dx_1 dx_2} = \frac{4\pi\alpha^2}{9sx_1x_2} \sum_i e_i^2 (q_i^B(x_1, Q^2)\bar{q}_i^T(x_2, Q^2) + \bar{q}_i^B(x_1, Q^2)q_i^T(x_2, Q^2)), \quad (1)$$

$s$  is the square of the center of mass energy and is given by  $s = 2m_T * E_{Beam} + m_T^2 + m_B^2$ , with  $E_{Beam}$  the beam energy and  $m_{B,T}$  the rest masses of the beam and target nucleons. Measuring the two decay leptons in the spectrometer allows one to determine the photon center of mass  $p_{\parallel}^{\gamma}$  (longitudinal) and  $p_T^{\gamma}$  (transverse) momenta as well as the mass  $M_{\gamma}$ . From these quantities one can deduce the momentum fractions of the quarks through:

$$x_F = \frac{p_{\parallel}^{\gamma}}{p_{\parallel}^{\gamma, max}} = x_1 - x_2, \quad sx_1x_2 = M_{\gamma}^2. \quad (2)$$

If one chooses the kinematics of the experiment such that  $x_F > 0$  and  $x_1$  is large, the contributions from the valence quarks in the beam dominate.

In this case, in Eq. 1 the second term becomes negligible and the cross section can be written as

$$\frac{d\sigma}{dx_1 dx_2} \approx \frac{4\pi\alpha^2}{9sx_1x_2} \sum_i e_i^2 q_i^B(x_1, Q^2)\bar{q}_i^T(x_2, Q^2). \quad (3)$$

For a proton beam on a proton target the process is dominated by the  $u(x_1)$  distribution due to the charge factor  $e_i^2$ . To extract the  $\bar{d}(x)$  Siverts asymmetry one has to measure the  $p+d^{\uparrow}$  asymmetry. In the following discussion we will assume that the cross section on the deuteron is the sum of the proton and neutron cross sections and use isospin symmetry to equate  $\bar{d}_p$  and  $\bar{u}_n$  and ignore strange and heavier antiquarks in the target, as well as antiquarks in the beam. Through a simultaneous measurement of the  $pp^{\uparrow}$  and  $pd^{\uparrow}$  asymmetries one can independently extract the Siverts asymmetry for both  $\bar{u}$  and  $\bar{d}$ .

## 2.2 Theory

The fundamental importance of studying transverse momentum dependent parton distributions (TMDs) and advancing the related theory of the nucleon spin is well summarized by the goals of the nuclear theory TMD Topical Collaboration, where LANL is a key member [21]. The study

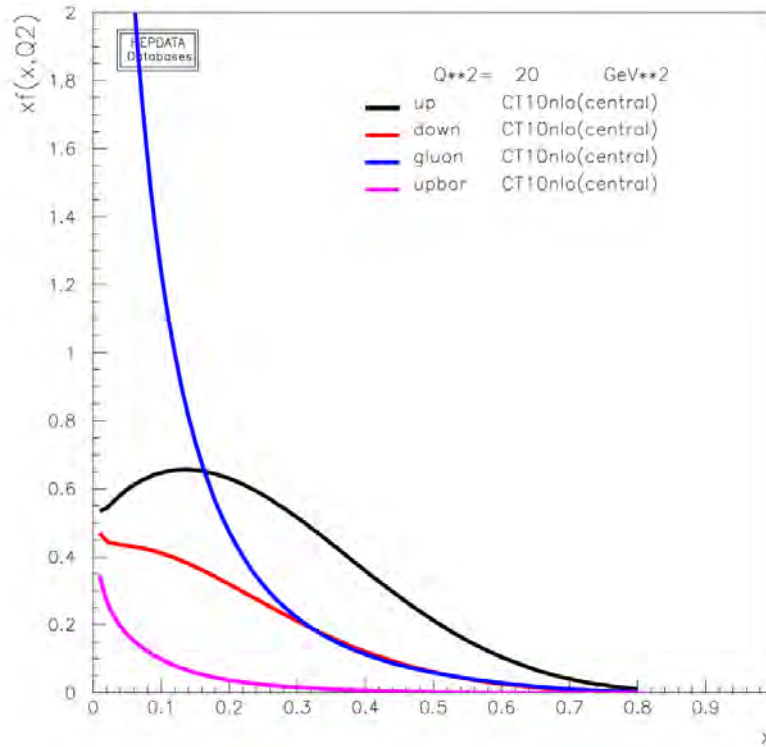


Figure 7: *The CTEQ10 parton distributions*

of TMDs is also one of the main focus areas for the future Electron Ion Collider (EIC) [3]. The theoretical motivation is briefly discussed below.

Nucleons (protons and neutrons) are the fundamental building blocks of atomic nuclei and make up essentially all the visible matter in the universe. Our modern understanding of the strong interaction is based on Quantum Chromodynamics (QCD), in which the nucleon arises as a strongly interacting, relativistic bound state of quarks and gluons (referred to as partons). The nucleon is not static, but has complex internal structure, full of features that ultimately emerge from QCD dynamics and that are only now beginning to be revealed in modern experiments. Explaining the origin, the evolution, and the structure of the visible world is a central goal of nuclear physics. In order to do this, it is vital to understand the internal structure of the nucleon in terms of its partonic constituents.

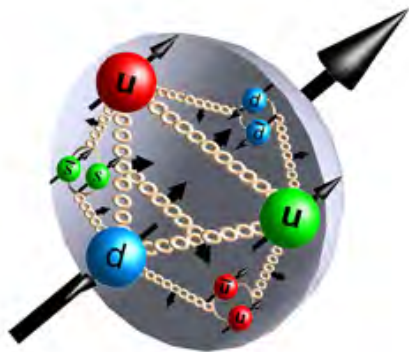


Figure 8: *Proton as a dynamical system of quarks and gluons.*

Over the last 50 years, since the first deep inelastic scattering experiments, there have been many advances in our understanding of the partonic structure of the nucleon, including its momentum and spin structure. The most significant progress has been in understanding the (*one-dimensional*) longitudinal momentum distributions of quarks and gluons encoded in the standard unpolarized collinear parton distribution functions (PDFs)  $f_1(x, Q)$  (see Fig. 7), with  $x$  the longitudinal momentum fraction of the nucleon carried by the parton and  $Q$  the resolution momentum scale of the external probe. However, there are still unknown and important aspects of the nucleon structure to be further explored, especially the ones related to the transverse momentum distribution of partons and its full 3-dimensional landscape (both *longitudinal* and *transverse* dimensions), Fig. 8. With the running of the COMPASS experiment at CERN, RHIC at BNL, the E906/SeaQuest Drell-Yan experiment at Fermilab,  $e^+e^-$  annihilation experiments at Belle and BaBar, and experiments at JLab, we have uncovered the first layers of transverse partonic structure of the proton. It is critical to ramp up the experimental investigation of TMDs and provide accurate and thus far missing experimental information on polarized proton reactions to enable important advances in our understanding of QCD dynamics and nucleon structure.

### 2.2.1 TMDs

Transverse momentum dependence in the parton distributions of the nucleon allows for the appearance of unsuppressed single spin azimuthal asymmetries, such as Sivers [7] and Collins [18] asymmetries. In turn, the measured spin azimuthal asymmetries will enable us to extract the TMD parton distributions through a global analysis of the experimental data, from which we can obtain an “image” of the nucleon in transverse, as well as in longitudinal momentum space (2+1 dimensions). Quark TMDs can be defined through the so-called quark-quark correlation function in the nucleon as follows:

$$\Phi^q(x, \vec{p}_T, S) = \int \frac{dz^- d^2\vec{z}_T}{(2\pi)^3} e^{ip^+z^- - i\vec{p}_T \cdot \vec{z}_T} \langle P, S | \bar{\psi}^q(0) \psi^q(z) | P, S \rangle, \quad (4)$$

$$= \Phi^{q[\gamma^+]} \frac{\gamma^-}{2} + \Phi^{q[\gamma^+\gamma^5]} \frac{\gamma^5 \gamma^-}{2} + \Phi^{q[i\sigma^{\alpha+}\gamma^5]} \frac{i\sigma^{-\alpha}\gamma^5}{2}. \quad (5)$$

Here  $\alpha$  is a transverse index, and  $\Phi^{q[\Gamma]} \equiv \frac{1}{2} \text{Tr}[\Phi^q \Gamma]$  for the specific Dirac matrix  $\Gamma$  as given above, from which we can write down all the *eight* quark TMDs in the following way:

$$\Phi^{q[\gamma^+]} = f_1^q(x, \vec{p}_T^2) - \frac{\epsilon_T^{ij} p_T^i S_T^j}{M} f_{1T}^{\perp q}(x, \vec{p}_T^2), \quad (6)$$

$$\Phi^{q[\gamma^+\gamma^5]} = S_L g_{1L}^q(x, \vec{p}_T^2) + \frac{\vec{p}_T \cdot \vec{S}_T}{M} g_{1T}^q(x, \vec{p}_T^2), \quad (7)$$

$$\begin{aligned} \Phi^{q[\sigma^{\alpha+}\gamma^5]} &= S_T^\alpha h_{1L}^q(x, \vec{p}_T^2) + \frac{p_T^\alpha (\vec{p}_T \cdot \vec{S}_T) - \frac{1}{2} \vec{p}_T^2 S_T^\alpha}{M^2} h_{1T}^{\perp q}(x, \vec{p}_T^2) \\ &\quad + S_L \frac{p_T^\alpha}{M} h_{1L}^{\perp q}(x, \vec{p}_T^2) + \frac{\epsilon_T^{ij} p_T^i S_T^j}{M} h_{1T}^{\perp q}(x, \vec{p}_T^2), \end{aligned} \quad (8)$$

where  $S_T$  and  $S_L$  are the transverse and longitudinal polarization vector of the nucleon.

It might be worth mentioning several important TMDs, which are directly relevant to our experiment. The “simplest” TMD is the unpolarized function  $f_1^q(x, \vec{p}_T^2)$ , which describes, in a fast moving nucleon, the probability of finding a quark carrying the longitudinal fraction  $x$  of the nucleon momentum, and a transverse momentum  $p_T = |\vec{p}_T|$ . It is related to the collinear

Leading Twist TMDs ○ → Nucleon Spin ⊙ → Quark Spin

		Quark Polarization		
		Un-Polarized (U)	Longitudinally Polarized (L)	Transversely Polarized (T)
Nucleon Polarization	U	$f_1 =$		$h_1^\perp =$ Boer-Mulders
	L		$g_{1L} =$ Helicity	$h_{1L}^\perp =$
	T	$f_{1T}^\perp =$ Sivers	$g_{1T}^\perp =$	$h_1 =$ Transversity

Figure 9: Classification of the quark TMDs. Table taken from Ref. [3]. Note that in the table the superscript  $q$  is omitted since it is understood that this table refers to quark TMDs.

PDF through  $\int d^2\vec{p}_T f_1^q(x, \vec{p}_T^2) = f_1^q(x)$ . Other TMDs that *do not* vanish when integrated over the transverse momentum are the helicity  $g_{1L}^q(x, \vec{p}_T^2)$  and transversity  $h_1^q(x, \vec{p}_T^2)$ . The most important TMD for our experiment is certainly the quark Sivers function  $f_{1T}^{\perp q}(x, \vec{p}_T^2)$ , which describes the distribution of unpolarized quarks inside a transversely polarized nucleon, through a correlation between the quark transverse momentum  $\vec{p}_T$  and the nucleon transverse spin  $S_T$ . It is time-reversal odd. Another naively time-reversal odd distribution is the Boer-Mulders function  $h_1^{\perp q}(x, \vec{p}_T^2)$ . All the quark TMDs can be classified through the polarizations of the nucleon and the quark inside the nucleon, as given by Fig. 9.

Of all these TMDs, the Sivers function has garnered considerable interest from both experimental and theoretical communities in QCD and hadron physics. The study of the Sivers function (as well as other TMDs) has challenged and greatly improved our understanding of the interplay between hadron structure and the process in which this structure is probed. The Sivers function has been measured in semi-inclusive deep inelastic polarized lepton-proton ( $\ell + p^\uparrow$ ) scattering experiments (SIDIS) by HERMES, COMPASS, and JLab, and will continue to be explored in the future at the EIC. It can also be readily measured in polarized proton-proton ( $p + p^\uparrow$ ) collisions through Drell-Yan production. Our proposed measurement of the Sivers function with E1039 in polarized DY reactions can provide critical information for the following questions of great experimental and theoretical significance:

- *What is the magnitude and sign of the sea quark Sivers function and how does it compare to the sign and magnitude in the valence quark region?*

Current SIDIS experiments allow for the accurate extraction of the Sivers function in the valence quark region. At smaller Bjorken  $x$ , where sea quarks dominate, the uncertainty through global fitting becomes large. The lack of experimental data forces the fits to zero and the systematic uncertainties cannot be properly evaluated. See for example Fig. 10.

- *What is the relation of the Sivers asymmetry measured in SIDIS to the one measured in the DY process, especially in the sea quark dominant region?*

It is a fundamental prediction of QCD that the Sivers function should change sign in going from SIDIS to DY,

$$f_{1T}^{\perp q \text{ DY}}(x, \vec{p}_T^2) = -f_{1T}^{\perp q \text{ SIDIS}}(x, \vec{p}_T^2). \quad (9)$$

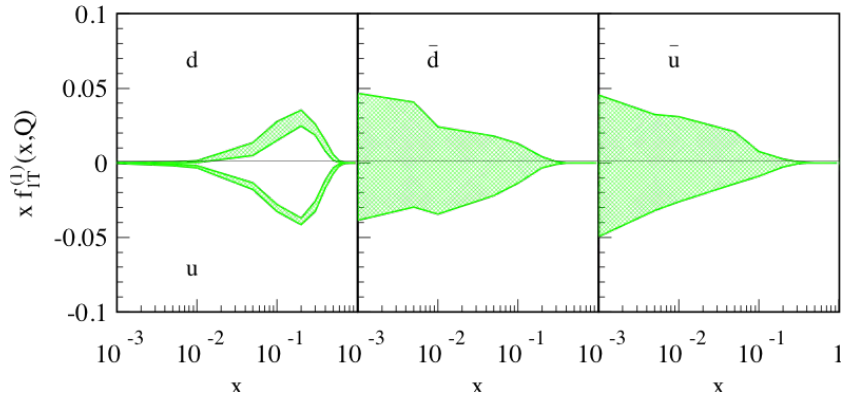


Figure 10: *Example of extraction of quark TMDs via global fitting from Ref. [25]. Shown is the collinear Qiu-Sterman function, related to the first  $p_T^2$  moment of the quark Sivers TMD. Note the relatively small error band for valence quarks and the large error band for sea quarks.*

The E1039 experiment will provide unique information for the sea quark Sivers function in DY that will help validate and advance QCD theory of TMDs. Even with input from a relatively recent analysis of the Sivers asymmetry in SIDIS [25], the sign of the Sivers asymmetry in DY cannot be determined due to the largely unknown sea quark Sivers functions. As shown in Fig. 11, the large uncertainty is in the region of  $x_F \in (-0.2, 0.6)$ , where E1039 measurements are sensitive and thus can make unique contributions. On the other hand, future measurements at the EIC will help determine the sea quark Sivers function in SIDIS. Combining both measurements, one can provide the important check for the fundamental prediction of sign change, particularly, for sea quark Sivers function.

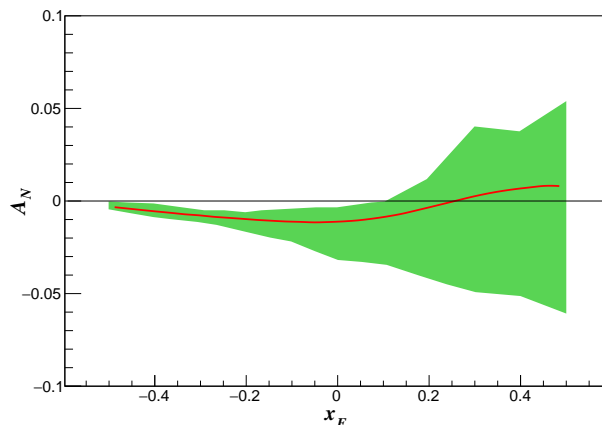


Figure 11: *Uncertainties in the predicted Sivers asymmetry in polarized Drell-Yan reactions. The Fermilab E1039 acceptance is for Feynman  $x_F \in (-0.2, 0.6)$ . Negative  $x_F$  is dominated by the known valence quark Sivers asymmetry, while positive  $x_F$  is dominated by the unknown sea quark Sivers asymmetry.*

- *What is the QCD evolution of the TMDs?*

QCD provides very powerful predictions concerning the dependence (evolution) of the TMD denoted generically as  $f(x, \vec{p}_T^2; Q)$  on the hard scale  $Q$  of the physical process [25, 26, 27, 28], through the so-called TMD factorization theorems [29, 31, 32]. Over the past decades TMD

factorization formalism has been greatly improved using various approaches, see Refs. [33, 34, 35, 36]. A unique feature of the TMD evolution distinctive from the usual collinear QCD evolution is the dependence on the non-perturbative aspects of gluon radiation. This can be easily seen as follows: assuming one starts from a TMD  $f(x, \vec{p}_T^2; Q_i)$  measured at a lower scale  $Q_i$ , and evolve to a TMD  $f(x, \vec{p}_T^2; Q_f)$  at a higher scale  $Q_f$ , the QCD evolution kernel should depend on  $x, \vec{p}_T^2, Q_i, Q_f$  and is thus denoted as  $R(x, \vec{p}_T^2, Q_i, Q_f)$ . As long as  $p_T$  can be as small as  $\Lambda_{\text{QCD}}$ , which is the relevant region for TMDs, we are faced with a non-perturbative contribution to the TMD evolution kernel.

Because of this, to understand the QCD evolution of TMDs and thus to extract TMDs in much better precision, it is essential to have experimental measurements at multiple scales. Current SIDIS measurements probe the low  $Q^2$  (few  $\text{GeV}^2$ ) and  $Q_T < 1 \text{ GeV}$  region, while  $W/Z$  production in  $p + p^\uparrow$  collisions probes the very high  $Q^2 \simeq 100^2 \text{ GeV}^2$  and  $Q_T$  up to the 10  $\text{GeV}/c$  region. On the other hand, Drell-Yan measurements above the  $J/\psi$  peak fall in a unique region with  $Q^2$  in the range of  $4^2 < M^2 < 9^2 \text{ GeV}^2$  and  $Q_T \leq \text{few GeV}$ . The E1039 results will thus be highly complementary to those measurements for SIDIS and for  $W/Z$  production, and be critical to constrain the QCD evolution of TMDs.

## 2.2.2 Orbital Angular Momentum

There is compelling experimental evidence that the quark intrinsic angular momentum only contributes  $\sim 1/3$  of the proton spin. The majority of the proton spin is thus unaccounted for, which has been referred to as the ‘‘proton spin crisis’’ [37]. With recent experimental data from RHIC, it is fair to say that the sum of both quark and gluon spin contributions still cannot account for the total proton spin [38]. The missing fraction of the spin (*potentially very large*) is likely to be carried by the orbital angular momentum (OAM) of the quarks and gluons.

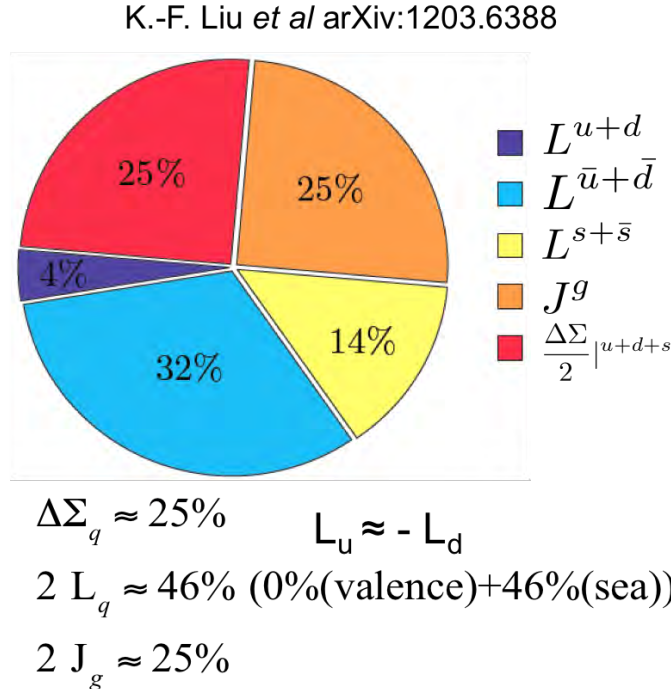


Figure 12: Various contributions to the orbital angular momentum of nucleons as given by a calculation of K.F. Liu *et al.* [48].

Recent theoretical developments have provided important insight into the decomposition of the nucleon spin into its quark and gluon contributions and further separation of these into spin and orbital components [46]. One such decomposition given by Ji [47] is

$$\frac{1}{2} = S_q + L_q + J_g. \quad (10)$$

The quark *total* angular momentum  $J_q = S_q + L_q$  can be obtained through an integral over the generalized parton distributions (GPDs), which can be extracted from exclusive scattering processes in  $\ell + p$  collisions, such as deeply virtual Compton scattering (DVCS). Combined with the longitudinal polarized DIS experimental data (for extraction of  $S_q$ ), one can thus determine the quark OAM  $L_q$ .

Another independent but complementary way to extract the information on  $L_q$  is through TMDs. Even though there is no established model-independent relation between TMDs and  $L_q$  [3, 39] nevertheless, most TMDs (including Sivers) would vanish in the absence of parton OAM, and thus enable us to extract important information about the quark OAM from the measurements of TMDs. The extraction of the sea quark Sivers functions can uniquely determine whether the sea quark OAM vanishes or not. At the same time, one can quantify the amount of the sea quark OAM although one relies on some model ansatz (well-motivated), see, e.g., Ref. [40].

Finally, another promising way forward is to use lattice QCD calculations to evaluate the individual contributions to the nucleon spin. One such calculation is shown in Fig. 12, where the OAM is dominantly carried by sea quarks [48]. The contributions from valence  $u$  and  $d$  quarks come with opposite sign and cancel each other. This is similar to the sign difference of the Sivers function for  $u$  and  $d$  quarks found from global extractions, see for example Fig. 10. Phenomenologically one can establish a relation between the strength of the Sivers functions and lattice QCD results and use this relation as a guidance to assess the sea quark contribution to the OAM. For the recent lattice calculations of the quark Sivers functions, see, Ref. [41].

## 2.3 Current theoretical and experimental status

Semi-Inclusive Deep Inelastic Scattering (SIDIS) experiments at HERMES [12], COMPASS [13], and JLab [14] have observed non-zero values of the Sivers function. The data indicate that the orbital angular momentum of the up quarks is positive ( $L_u > 0$ ) and that of the down quarks is negative ( $L_d < 0$ ), and of similar magnitude. Due to this cancellation, the valence quarks may carry little net orbital angular momentum. This result is confirmed by Lattice QCD calculations [48]. Echevarria, *et al* [25], have performed a global fit of the Sivers data from SIDIS. They found that while the valence quark Sivers function are well constrained and opposite for  $u$  and  $d$  quarks, those for the sea quarks are largely unconstrained.

Further insight into the orbital angular momentum contribution for the sea quarks requires the use of two body reactions with an antiquark in the initial state. These include the Drell-Yan reaction (Fig. 6) and production of  $W$  and  $Z$  bosons. Due to their large masses, the  $W$  and  $Z$  measurements are only feasible at high energy collider facilities. Small asymmetries cannot usually be observed, due to limited statistics. The STAR experiment at RHIC has published transverse single spin asymmetries for  $W$ 's [49]. While the statistics are quite limited, the asymmetries appear to be non-zero and positive for both  $W^+$  and  $W^-$ . STAR plans to collect up to 5X more data in the near future and may be able to observe the Sivers sign change versus SIDIS. While the  $W$  and  $Z$  measurements probe a combination of the Sivers function and the parity violating transverse

helicity distribution, as mentioned previously, they are also carried out at much higher  $Q^2$ . Drell-Yan production on fixed target experiments typically has higher integrated luminosity and are carried out at a lower  $Q^2$ . The COMPASS experiment at CERN [13] has performed transverse single spin asymmetry measurements, with first results expected during this year. Due to the presence of the antiquark in the pion beam, COMPASS is primarily sensitive to valence quarks in the polarized target. Additional information summarizing the polarized Drell-Yan experiments at various laboratories around the world is given in Section 4 below.

Thus, no existing experiment is capable of directly measuring the Sivers asymmetry of the sea quarks with high precision. Our proposed E1039 experiment is based upon the proven E906 spectrometer, which has already acquired large numbers of Drell-Yan events from liquid hydrogen and deuterium. LANL and UVa have recently completed and tested a new transversely polarized proton target capable of both high polarization and integrated luminosity. We note that the E1027 experiment at FNAL would instead use a transversely polarized beam with the E906 experiment, to measure the valence quark Sivers function, with a better figure of merit than COMPASS. Another unique capability of E1039 is the ability to separately measure the Sivers function for the  $\bar{d}$  and  $\bar{u}$  quarks using polarized  $\text{NH}_3$  and  $\text{ND}_3$  targets.

There are a few theoretical estimates available for the magnitude of the Sivers asymmetry in Drell-Yan, based on global fits to the existing SIDIS data. Anselmino, *et al* [59] and Sun and Yuan [28] predict central Sivers values ranging from 0. to 0.2 but have very large uncertainties, as shown in Fig. 22. More recently, Echevarria, *et. al.* [25], have confirmed that the fits to the existing data are rather insensitive to contributions from the antiquarks, as shown in Fig. 10. Lattice QCD calculations predict a large net orbital angular momentum contribution from the sea quarks [48].

## 2.4 The angular dependence of the Drell-Yan cross section

When studying the angular dependence of the proton induced Drell-Yan process,  $pp^\uparrow \rightarrow \mu^+\mu^-$ , three angles are of relevance: the azimuthal angle  $\phi_S$  of the transverse spin orientation  $\mathbf{S}_T$  of the target (determined in the target rest frame) and the polar and azimuthal angles  $\theta$  and  $\phi$  of the dimuon pair (determined in the Collins-Soper frame [29], i.e. the dimuon center-of-mass system). The definition of the angles  $\theta$  and  $\phi$  is shown in Fig. 2. In the one-photon approximation, the differential cross section through the orientation  $d\Omega$  of the dimuon pair can be decomposed in a

model-independent way [30] such that

$$\begin{aligned}
\frac{d\sigma}{d^4q d\Omega} &= \frac{\alpha^2}{4q^2 \sqrt{(P_b \cdot P_t)^2 - M_p^2}} \\
&\left\{ \begin{aligned} &\left[ (1 + \cos^2 \theta) F_{UU}^1 + (1 - \cos^2 \theta) F_{UU}^2 \right. \\ &\quad \left. + \sin 2\theta \cos \phi F_{UU}^{\cos \phi} + \sin^2 \theta \cos 2\phi F_{UU}^{\cos 2\phi} \right] \\ &+ S_L \left[ \sin 2\theta \sin \phi F_{UL}^{\sin \phi} + \sin^2 \theta \sin 2\phi F_{UL}^{\sin 2\phi} \right] \\ &+ S_T \left[ \sin \phi_S \left( (1 + \cos^2 \theta) F_{UT}^1 + (1 - \cos^2 \theta) F_{UT}^2 \right. \right. \\ &\quad \left. \left. + \sin 2\theta \cos \phi F_{UT}^{\cos \phi} + \sin^2 \theta \cos 2\phi F_{UT}^{\cos 2\phi} \right) \right. \\ &\quad \left. \left. + \cos \phi_S \left( \sin 2\theta \sin \phi F_{UT}^{\sin \phi} + \sin^2 \theta \sin 2\phi F_{UT}^{\cos 2\phi} \right) \right] \right\}. \tag{11}
\end{aligned}
\end{aligned}$$

Here, only partial cross sections are included where the polarization component  $S_T$  ( $S_L$ ) of the target is transverse (longitudinal) to the direction of the virtual photon. The structure functions  $F(P_b \cdot q, P_t \cdot q, q \cdot q)$  depend on three independent Lorentz scalars calculated from the beam, target and virtual photon momenta  $P_b$ ,  $P_t$  and  $q$ . Their first and second subscripts indicate, respectively, the beam and target polarizations ((U)nnpolarized, (L)ongitudinally polarized, (T)ransversely polarized). The related azimuthal modulation is given in a superscript. The Siverts mechanism manifests itself in a  $\sin \phi_S (1 + \cos^2 \theta)$  modulation in the cross section.

For small transverse momentum of the virtual photon,  $q_T \ll q$ , the process-dependent structure functions can be interpreted as convolution in transverse momentum space of the universal quark and antiquark distributions of beam and target. At leading twist accuracy and at leading order in  $\alpha_S$ , the structure function  $F_{UT}^1$  provides a signal for the Siverts TMD  $\bar{f}_{1T}^\perp$  in conjunction with the well-known polarization-averaged PDF  $f_1$  of valence quarks such that

$$F_{UT}^1 = -\mathcal{C} \left[ \frac{\mathbf{q}_T \cdot \mathbf{k}_{T,b}}{q_T M_p} f_1(x_t, \mathbf{k}_{T,b}^2) \bar{f}_{1T}^\perp(x_b, \mathbf{k}_{T,t}^2) \right]. \tag{12}$$

Here, the convolution over the intrinsic transverse momenta  $\mathbf{k}_T$  of the quark and antiquark is represented by the symbol  $\mathcal{C}$ .

The Siverts function can be experimentally constrained by a measurement of the angular distribution of dimuon pairs produced in the Drell-Yan process with a transversely polarized target. The structure function  $F_{UT}^1$  is revealed in a  $\sin \phi_S (1 + \cos^2 \theta)$  signature.

In the following we present the simple expression extracting the asymmetry in LO. Taking into account the dilution factor  $f$ , which describes the ratio of polarizable nucleons over the total number of nucleons, and integrating over the virtual photon transverse momentum  $p_T$  and the lepton pair angle  $\Theta$  we can write the number of events in a  $x_b$  and  $x_T$  bin as :

$$\begin{aligned}
\frac{dN(x_b, x_T, \phi, \phi_S)}{d\phi d\phi_S} &= N(x_b, x_T) \left\{ \left( 1 + \frac{1}{2} A_{UU}^{\cos 2\phi} \cos 2\phi \right) \right. \\ &+ f S_L \frac{1}{2} A_{UL}^{\sin 2\phi} \sin 2\phi \\ &+ f |S_T| \left[ A_{UT}^{\sin \phi_S} \sin \phi_S + \frac{1}{2} \left( A_{UT}^{\sin(2\phi+\phi_S)} \sin(2\phi + \phi_S) \right. \right. \\ &\quad \left. \left. + A_{UT}^{\sin(2\phi-\phi_S)} \sin(2\phi - \phi_S) \right) \right] \left. \right\} \tag{13}
\end{aligned}$$

Using the Fourier projection on the  $\sin \phi_S$  modulation finally gives

$$A_{UT}^{\sin \phi_S} = \frac{2}{f|S_T|} \frac{\int d\phi_S d\phi \frac{dN(x_b, x_T, \phi, \phi_S)}{d\phi_S d\phi} \sin \phi_S}{N(x_b, x_T)}. \quad (14)$$

This asymmetry is then connected to the structure function in Eq. 12

$$A_{UT}^{\sin \phi_S} = \frac{F_{UT}^1}{F_{UU}^1}. \quad (15)$$

where the structure function  $F_{UU}^1$  can be interpreted as a convolution in transverse momentum space of the polarization averaged PDF for quarks and for antiquarks.

## 2.5 The Measurements

For the purpose of the proposed measurements, one needs to separately measure the Sivers function for  $\bar{u}$  and  $\bar{d}$  quarks. The approach we will follow is similar to that used previously by experiments E866 and E906 to measure the  $\bar{d}/\bar{u}$  ratio in the proton. A transversely polarized proton target is necessary for the  $\bar{u}$  Sivers measurement, where the dominant Drell-Yan channel is a valence  $u$  quark from the unpolarized proton beam annihilating with a  $\bar{u}$  (sea) quark from the target to form the virtual photon. A transversely polarized deuteron target is used for the  $\bar{d}$  Sivers measurement, with the neutron providing additional  $\bar{d}$  assuming iso-spin symmetry.

A simultaneous measurement of the Sivers function for gluons is also possible with the polarized proton target. Production of the  $J/\psi$  meson (a charmonium state) at small  $x_F$  is primarily due to gluon-gluon fusion. The  $J/\psi$  cross section and dimuon decay branch are large while the mass of 3.097 GeV places it well within our experimental acceptance. This gluon Sivers measurement requires no hardware changes to the experiment and is discussed further in Appendix C.2.

### 2.5.1 $p + p^\uparrow$

A dynamically polarized  $\text{NH}_3$  target is the optimum choice for a transversely polarized proton target. While the dilution factor is small (0.18), due to the presence of a nitrogen atom, large polarization values of greater than 95% for the protons can be obtained. Measurement of Drell-Yan events at forward rapidity (positive  $x_F$ ) naturally selects  $u(\text{beam}) + \bar{u}(\text{target})$  with only a small background from other quark combinations. The Sivers asymmetry is constructed from the normalized difference of the cross sections for events with opposite target polarization. Most of the systematic errors can be canceled by reversing the target polarization or the magnetic fields of the spectrometer. The expected statistical error for a 1-yr  $\text{NH}_3$  measurement is  $\sim 3\%$  for the central  $x_2$  bins, while the systematic error is less than 1%.

### 2.5.2 $p + d^\uparrow$

$\text{ND}_3$  can be used to provide the transversely polarized neutron target. Here the dilution factor is higher (0.3), with a maximum polarization of up to 50%, leading to similar sensitivity as for the  $\text{NH}_3$  target. As for the proton target, events at forward rapidity select primarily sea quarks. The additional neutron in the deuteron increases the sensitivity to  $\bar{d}$  under the assumption of iso-spin symmetry. The Sivers  $\bar{d}$  asymmetry is extracted from a comparison of the measured proton and deuteron asymmetries. The expected statistical error for a 1-yr  $\text{ND}_3$  measurement is 4% for the

central  $x_F$  bins, with a systematic error of less than 1%. Use of  $\text{ND}_3$  requires some changes to our existing polarized target. The Larmor (spin flip) frequency for deuterium is much lower than for hydrogen, 32 MHz versus 213 MHz, respectively, requiring a small modification of the NMR system used to measure the polarization.

Since the deuteron is a spin 1 nucleus, both vector and tensor polarizations are available. Thus, a measurement of the tensor structure function  $b_1$  is possible with the  $\text{ND}_3$  target as is discussed further in Appendix C.1.

### 3 Experimental Setup

#### 3.1 The Spectrometer

We are proposing to use the existing E906/SeaQuest [50] spectrometer shown in Fig. 13 to perform our measurement. The spectrometer consists of two magnets, FMAG and KMag, and four tracking stations, where the last one serves as a muon identifier. It was designed to perform Drell-Yan measurements at large  $x_1$ . This is illustrated in Fig. 14, where the acceptance of E1039 is plotted as function of  $x_1$  (x-axis) and  $x_2$  (y-axis).

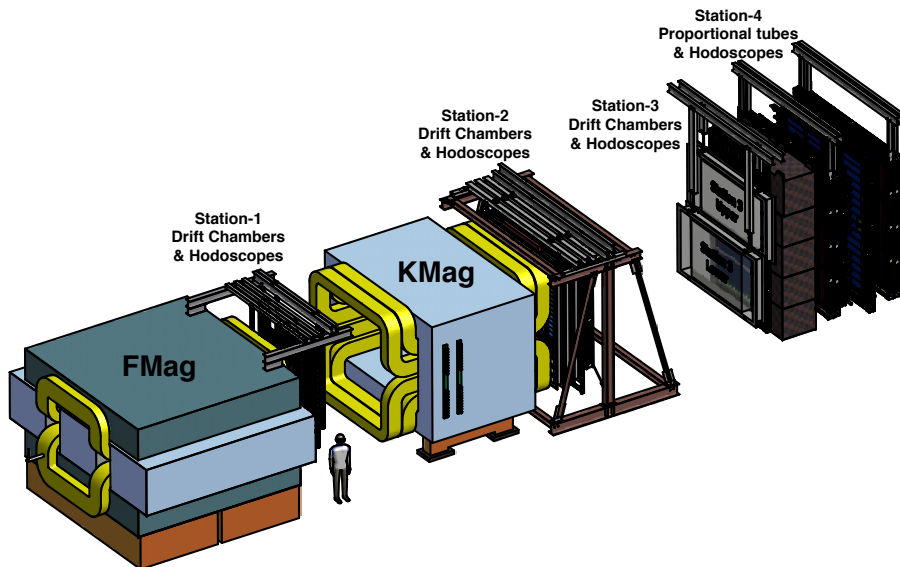


Figure 13: *The SeaQuest Spectrometer*

This is an excellent kinematic range for the proposed sea quark Siverson function measurement, covering the region of large anti-down quark excess observed by E866, where large pion-cloud effects may be expected. The contributions from target valence quarks at large  $x_2$  are then negligible as can be seen from Fig. 7.

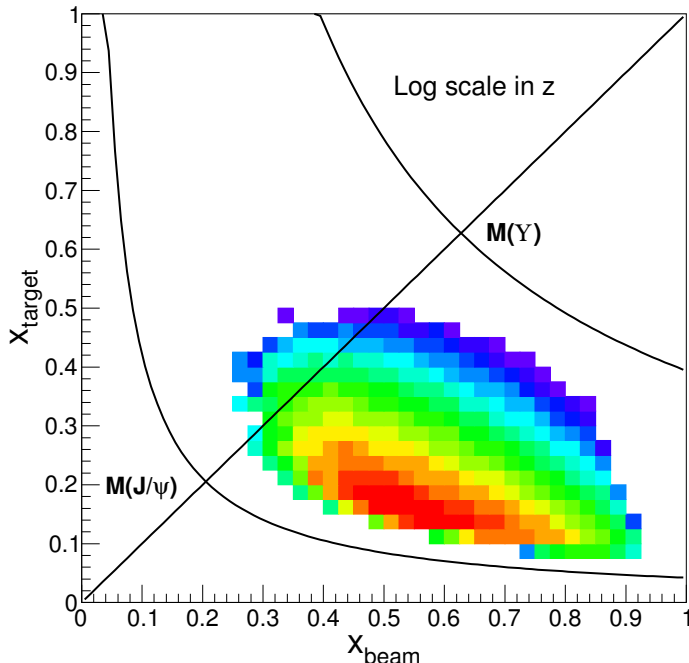


Figure 14: *The kinematic acceptance of the E1039 experiment.*

The experiment will be using the Fermilab main injector beam with an energy of 120 GeV and a 4 second spill every minute. The maximum beam intensity will be  $\simeq 10^{13}$  protons per spill.

### 3.2 The Polarized Target

We will use the LANL-UVa polarized target which has been rebuilt and tested over the last three years. The target system consists of a 5T superconducting split coil magnet, a  $^4\text{He}$  evaporation refrigerator, a 140 GHz microwave source and a large 15000  $\text{m}^3/\text{hr}$  pumping system. The target is polarized using Dynamic Nuclear Polarization (DNP) [52] and is shown schematically in Fig. 15. The beam direction is from left to right, and the magnetic field is vertical along the symmetry axis, so that the target polarization is transverse to the beam direction. The target cells are shown in gold color, with the top cell in the center of the split coils. The full system is shown in Fig. 16.

While the magnetic moment of the proton is too small to lead to a sizable polarization in a 5 T field, electrons in that field at 1 K are better than 99% polarized. By doping a suitable solid target material with paramagnetic radicals to provide unpaired electron spins, one can make use of the highly polarized state of the electrons. The dipole-dipole interaction between the nucleon and the electron leads to hyperfine splitting, providing the coupling between the two spin species. By applying a suitable microwave signal, the desired spin state is populated. We will use frozen ammonia beads of  $\text{NH}_3$  and  $\text{ND}_3$  as the target material and create the paramagnetic radicals (roughly  $10^{19}$  spins/ml) through irradiation with a high intensity electron beam at the National Institute of Standards and Technology (NIST). The cryogenic refrigerator, which works on the principle of liquid  $^4\text{He}$  evaporation, can cool the bath to 1K, by lowering the  $^4\text{He}$  vapor pressure down to less than 0.118 Torr. The polarization will be measured with three NMR coils per cell, placed inside each target cell. The maximum polarization achieved with the proton (deuteron) target is better than 98% (48%) and the ammonia bead packing fraction is about 60%. In our

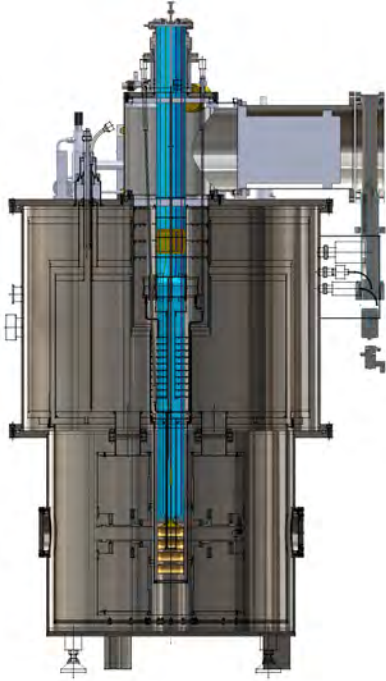


Figure 15: *Cross sectional drawing of the polarized target system*



Figure 16: *The LANL-UVa target during its full operations test in April 2016*

estimate for the statistical precision, we have assumed an average polarization of 80%. In the case of the deuteron target we have assumed 32% average polarization. The polarization dilution factor, which is the ratio of free polarized protons to the total number of nucleons, is 3/17 for  $\text{NH}_3$  and 3/10 for  $\text{ND}_3$ , due to the presence of nitrogen. The target material will need to be replaced approximately every 8 -10 days in all three cells, due to the beam induced radiation damage. This work will involve replacing the target stick with a new insert, cooling down the target and performing a thermal equilibrium measurement. From previous experience, we estimate that this will take about eight hours to accomplish. Careful planning of these changes will reduce the impact on the beam time. Furthermore, we will be running with three active targets on one stick, thus reducing any additional loss of beam time. The target cells are 79 mm long and elliptical with 21 mm  $\times$  19mm as vertical and horizontal axes. Each cell contains 3 NMR coils spaced evenly over the target length.

Material	Dens.	Dilution Factor	Packing Frac	$\langle \text{Pol} \rangle$	Inter. Length
$\text{NH}_3$	.867 g/cm <sup>3</sup>	.176	.60	80%	5.3 %
$\text{ND}_3$	1.007 g/cm <sup>3</sup>	.3	.60	32%	5.7%

Table 1: *Parameters for the polarized target*

### 3.3 Beamline

The Neutrino-Muon (NM) beamline currently supporting the E906 Drell Yan experiment delivers a high-intensity (up to  $10^{13}$  protons/4-sec spill), 120-GeV proton beam. The experimental beam has

the 53 MHz microbunch characteristics of the Fermilab Main Injector RF structure and the longer microsecond structure of consecutively injected Fermilab Booster beam batches -with appropriate intervening kicker gaps separating the injected batches. After traversing a lengthy beamline interspersed with vacuum windows and in-beam diagnostics such as Secondary Emission Monitors (SEMs), the beam is distinctly Gaussian with Lorentzian tails. These tails are problematic for the cryogenic coils that polarize the E1039 target. However, this beamline is uniquely suited to tailor and customize beam properties - upstream beam collimation allows both matching the beam profile to the dimensions of the polarized target vertically and horizontally and protection against a quench of the SC magnet without creating increased backgrounds at the experiment.

### 3.3.1 Current and Proposed Beamline Configuration

The beam is slow-spill extracted from the Fermilab Main Injector on the half integer resonance. Although slow spill produces an asymmetric, non-elliptical phase space in the horizontal plane, after traveling through vacuum windows, diagnostics, and other sources of scattering, the beam in both planes becomes Gaussian-like (with Lorentzian tails) and even symmetry. (The vertical split of beam to the MTEST and MCENTER lines is at such low intensity, that the beam profile in this high-intensity line is not observably impacted.)

The NM/E906 beam properties have been extensively studied to determine how to achieve the requested beam profile on the polarized target. A minimal spot size of  $\sigma = 3 - 4$  mm is the smallest obtainable in both planes simultaneously with the present beamline magnet configuration and distances involved (Fig. 17 and 18) - the polarized target is 2 meters upstream of the current E906 targets so these measurements apply. The new experiment has requested a spot size of 6 - 7 mm. No magnet reconfiguration or additions are required with beam collimation, greatly reducing the cost and lab resources required. The present beamline magnet configuration can thus be used for the E1039 experiment.

The primary modification required is to collimate beam by at least  $\sim 10-20\%$ , well upstream of the polarized target, to remove the potential for quenching the superconducting magnet and also to evenly distribute beam across the target. To do this the NM2 target pile from the kTeV experiment will be used to absorb beam scattered by collimators (Palmer-style) positioned upstream of this pile. These collimators are currently stored downstream of the target pile but can be rigged around the shielding and installed upstream replacing two of the 5 4Q120s (only the two last quadrupoles, 3 and 4 are currently in use for E906).

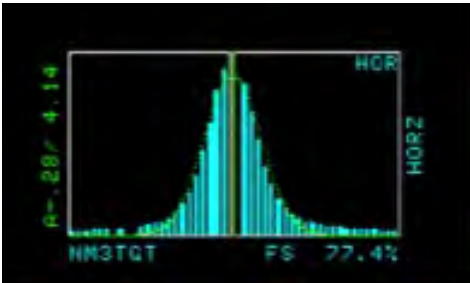


Figure 17: *Horizontal beam profile*

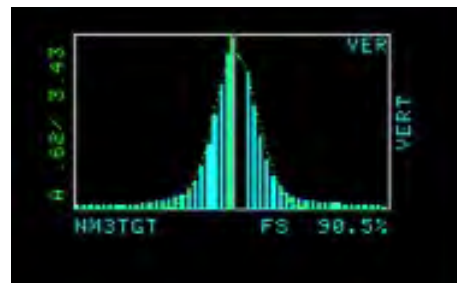


Figure 18: *Vertical beam profile*

By installing the collimators upstream, the beam can be collimated and tails clipped, scattered and completely absorbed by the NM2 target pile with little background reaching the experiment. A MARS study is planned for this configuration.

Finally, a fixed collimator in the NM3 enclosure will shadow the SC coils of the polarized target to protect it not only from any residual halo but also beam steering allowing target scans.

### 3.4 Integration of the polarized target into SeaQuest

### 3.5 Count Rates and Statistical Errors

The total Drell-Yan count rates on different targets are calculated using both full GEANT4 based Monte Carlo simulation program with Drell-Yan signal events generated by the NLO calculations done by Vitev, *et al*, and the demonstrated performance of the Fermilab Main Injector combined with the E906/SeaQuest spectrometer.

Unlike E906/SeaQuest, the primary physics interest of the E1039 experiment is to measure the low- $x_2$  range of polarized Drell-Yan production. We moved our target position from 130 cm to 300 cm upstream of the beam dump, which greatly improves the low- $x_2$  acceptance and the triggering capability, as well as the capability to separate target events from dump events.

One primary bottleneck of the data collection efficiency at E906/SeaQuest is the Data Acquisition System (DAQ). A very tight trigger level selection has been implemented in E906/SeaQuest so as to accommodate as many events in our limited DAQ bandwidth as possible. In the summer shutdown between Run-IV (FY-2016) and Run-V (FY-2017), we are upgrading our DAQ system to increase the bandwidth by a factor of up to 10, which will be available for the last run of E906/SeaQuest and following experiments.

Another limiting factor of the data collection efficiency at E906/SeaQuest was the unstable instantaneous beam intensity, which is sometimes more than one order of magnitude larger than average. To prevent the spectrometer from being completely saturated, the total number of protons delivered to the target was limited to less than  $6 \times 10^{12}$  per spill. This also requires the data taking to be inhibited on all neighboring RF buckets when a high intensity bucket arrives. After careful optimization, E906/SeaQuest has been able to record on average  $2.67 \times 10^{12}$  live protons per spill, which corresponds to  $7.7 \times 10^{17}$  protons per calendar year.

After running for 2 years with beam time evenly split between  $\text{NH}_3$  and  $\text{ND}_3$  targets (as shown in Table 2), the integrated luminosity on  $\text{NH}_3$  ( $\text{ND}_3$ ) target is expected to be  $1.82 \times 10^{42}$  ( $2.11 \times 10^{42}$ )  $\text{cm}^{-2}$ . With the various assumed efficiencies shown in Table 3, the final event yield and statistical precision of  $A_N$  measurement in each  $x_2$  bin is summarized in Table 4. Here the statistical precision is calculated by  $\Delta A_N = \frac{1}{f} \frac{1}{P} \frac{1}{\sqrt{N}}$ , where  $f$  denotes the dilution factor,  $P$  denotes the average polarization, and  $N$  denotes the event yield in each  $x_2$  bin.

Material	Dens. ( $\text{g}/\text{cm}^3$ )	Length (cm)	Interaction Length (cm)	Dilution Factor	Packing Fraction	$\langle P_z \rangle$	$\langle P_{zz} \rangle$
$\text{NH}_3$	0.867	7.9	91.7	0.176	0.6	80%	N/A
$\text{ND}_3$	1.007	7.9	82.9	0.3	0.6	32%	20%

Table 2: *Parameters for the polarized target*

Sources	Target/Accelerator	Spectrometer	Acceptance	Trigger	Reconstruction
Efficiency (%)	50	80	2.2	90	60

Table 3: *Various efficiencies assumed for the count rate estimates based on previous experience with E906 and polarized target operations.*

$x_2$ bin	$\langle x_2 \rangle$	$\text{NH}_3$ ( $p^\uparrow$ )		$\text{ND}_3$ ( $d^\uparrow$ )		$n^\uparrow$
		$N$	$\Delta A$ (%)	$N$	$\Delta A$ (%)	$\Delta A$ (%)
0.10 - 0.16	0.139	$5.0 \times 10^4$	3.2	$5.8 \times 10^4$	4.3	5.4
0.16 - 0.19	0.175	$4.5 \times 10^4$	3.3	$5.2 \times 10^4$	4.6	5.7
0.19 - 0.24	0.213	$5.7 \times 10^4$	2.9	$6.6 \times 10^4$	4.1	5.0
0.24 - 0.60	0.295	$5.5 \times 10^4$	3.0	$6.4 \times 10^4$	4.1	5.1

Table 4: *Event yield and statistical precision of the  $A_N$  measurement in each of the  $x_2$  bins for the  $\text{NH}_3$  ( $p^\uparrow$ ) and  $\text{ND}_3$  ( $d^\uparrow$ ) targets, and the deduced  $A_N$  measurement precision for polarized  $n$ .*

## 3.6 Polarization Measurements

### 3.6.1 Proton Polarization Measurements

The proton spin polarization is measured with a continuous-wave NMR system based on the Liverpool Q-meter design [51] and recently upgraded at LANL. The Q-meter works as part of a circuit with phase sensitivity designed to respond to the change of the impedance in the NMR coil. The radio-frequent (RF) susceptibility of the material is inductively coupled to the NMR coil which is part of a series LCR circuit, tuned to the Larmor frequency of the nuclei being probed. The output, consisting of a DC level digitized and recorded as a target event [52] in the target data acquisition system.

The polarized target NMR and data acquisition includes the software control system, the Rohde & Schwarz RF generator (R&S), the Q-meter enclosure, and the target cavity insert. The Q-meter enclosure is a standard VME crate, containing a series of Q-meter circuit boards with separate connection cables which are used for different target cup cells during the experiment. The target material and NMR coil are held in polychlorotrifluoroethylene (Kel-F) cells with the whole target insert cryogenically cooled to 1 K. Kel-F is used because it contains no free protons.

The R&S generator produces a RF signal which is frequency modulated to sweep over the frequency range of interest. Typically, the R&S responds to an external modulation, sweeping linearly from 400 kHz below to 400 kHz above the Larmor frequency. The signal from the R&S is connected to the NMR coils within the target material. To avoid degrading reflections in the long connection from the NMR coil to the electronics, a standing wave can be created in the transmission cable by selecting a length of cable that is an integer multiple of the half-wavelength of the resonant frequency. This specialized connection cable is known as the  $\lambda/2$  cable and is a semi-rigid cable with a teflon based dielectric. The NMR coil consists of a set of loops made of 70/30 copper-nickel tube, which minimizes interaction with the proton beam. The coil opens up into an oval shape spanning approximately 2 cm inside the cup. It is possible to enhance the signal to noise ratio by taking multiple frequency sweeps and averaging the signals. A completion of the set number of sweeps results in a single target event with a time stamp. The averaged signal is integrated to obtain a NMR polarization area for that event. Each target event written contains all NMR system parameters and the target environment variables needed to calculate the final polarization.

A target NMR calibration measurement or Thermal Equilibrium measurement (TE) is used to find a proportionality relation to determine the enhanced polarization under a range of thermal conditions given the area of the “Q-curve” NMR signal at the same magnetic field. The magnetic moment in the external field results in a set of  $2J+1$  energy sublevels through Zeeman interaction,

where  $J$  is the particle spin. The TE natural polarization for a spin-1/2 particle is given by,

$$P_{TE} = \tanh\left(\frac{\mu B}{kT}\right), \quad (16)$$

coming from Curie's Law [54], where  $\mu$  is the magnetic moment in the external field of strength  $B$ ,  $k$  is the Boltzmann constant, and  $T$  the temperature. Measuring  $P_{TE}$  at low temperature increases stability and the polarization signal. This is favorable because the uncertainty in the NMR signal increases as the area of the signal decreases. In fact much of the polarization uncertainty comes from this measurement. The goal temperature used is  $\sim 1.4$  K.

The dynamic polarization value is derived by comparing the enhanced signal  $S_E$  integrated over the driving frequency  $\omega$ , with that of the TE signal:

$$P_E = G \frac{\int S_E(\omega) d\omega}{\int S_{TE}(\omega) d\omega} P_{TE} = GC_{TE} A_E, \quad (17)$$

and calibration constant defined as,

$$C_{TE} = \frac{P_{TE}}{A_{TE}}. \quad (18)$$

$P_E$  ( $A_E$ ) is the polarization (area) of the enhanced signal and  $P_{TE}$  ( $A_{TE}$ ) is the polarization (area) from the thermal equilibrium measurement. The uncertainty in the calibration constant,  $\delta C_{TE}/C_{TE}$ , can easily be calculated using the fractional error from  $P_{TE}$  and  $A_{TE}$ . The ratio of gains from the NMR card used during the thermal equilibrium measurement to the enhanced signal is represented as  $G$ . For more detail, see [53].

### 3.6.2 Neutron Polarization Measurements

The deuteron polarization will be monitored by the same LANL continuous wave NMR system as used for the proton with one small change. There are two means whereby the polarization can be extracted from the NMR signal: the area method and the peak-height method. We intend to use both.

First, the total area of the NMR absorption signal is proportional to the vector polarization of the sample, and the constant of proportionality can be calibrated against the polarization of the sample measured under thermal equilibrium conditions. This is the standard method used for polarized proton targets, but can be more problematic for deuteron targets. Typical conditions for the TE measurements are 5 T and 1.4 K, where the deuteron polarization is only 0.075%, compared to 0.36% for protons. This smaller polarization, along with quadruple broadening, makes the deuteron TE signal more difficult to measure with high accuracy. A cold NMR system can be used to improve the signal-to-noise ratio of the NMR signal [55].

The deuteron polarization can also be extracted from the shape of the NMR signal. The deuteron is a spin-1 nucleus with three magnetic substates,  $m = -1, 0, +1$ , and the NMR absorption signal lineshape is the sum of the two overlapping absorption lines consisting of the  $-1 \rightarrow 0$  and  $0 \rightarrow +1$  transitions. In the case of  $\text{ND}_3$ , the deuteron's electric quadrupole moment interacts with electric field gradients within the molecule and splits the degeneracy of the two transitions. The degree of splitting depends on the angle between the magnetic field and direction of the electric field gradient. The resultant lineshape, integrated over a sample of many polycrystalline beads has the form of a Pake doublet. It has been experimentally demonstrated that, at or near steady-state conditions, the magnetic substates of deuterons in dynamically polarized  $\text{ND}_3$  are

populated according to the Boltzmann distribution with a characteristic spin temperature  $T$  that can be either positive or negative, depending on the sign of the polarization.

When the system is at thermal equilibrium with the solid lattice, the deuteron polarization is known from:

$$P_z = \frac{4 + \tanh \frac{\mu B}{2kT}}{3 + \tanh^2 \frac{\mu B}{2kT}} \quad (19)$$

where  $\mu$  is the magnetic moment, and  $k$  is Boltzmann's constant. The vector polarization can be determined by comparing the enhanced signal with that of the TE signal (which has known polarization). This polarimetry method is typically reliable to about 5% relative.

Similarly, the tensor polarization is given by:

$$P_{zz} = \frac{4 + \tanh^2 \frac{\mu B}{2kT}}{3 + \tanh^2 \frac{\mu B}{2kT}} \quad (20)$$

From Eqs. 19 and 20, we find:

$$P_{zz} = 2 - \sqrt{4 - 3P_z^2} \quad (21)$$

In addition to the TE method, polarizations can be determined by analyzing NMR lineshapes as described in [57] with a typical 5-7% relative uncertainty. At high polarizations, the intensities of the two transitions differ, and the NMR signal shows an asymmetry  $R$  in the value of the two peaks. The vector polarization is then given by:

$$P_z = \frac{R^2 - 1}{R^2 + R + 1} \quad (22)$$

and the tensor polarization is given by:

$$P_{zz} = \frac{R^2 - 2R + 1}{R^2 + R + 1} \quad (23)$$

This measuring technique can be used as a compliment to the TE method resulting in reduced uncertainty in polarization for vector polarizations over 28%.

The measurement of the neutron polarization ( $P_n$ ) is achieved by a calculation using the NMR measured polarization of the deuteron ( $P_d$ ). The quantum mechanical calculation using Clebsch-Gordan coefficients show 75% of the neutron spins in the  $D$ -state are antiparallel to the deuteron spins [56]. The resulting neutron polarization is,

$$P_n = (1 - 1.5\alpha_D)P_d \approx 0.91P_d,$$

where  $\alpha_D$  is the probability of the deuteron to be in a  $D$ -state.

### 3.6.3 Target Polarization Uncertainty

The lower limit for polarization uncertainty is set by the Q-meter style NMR which can not be expected to perform better than 1% relative error. UVA test lab studies have gone down as far as 1.5% but typically in an experiment 2-4% is achieved for the proton. The Deuteron/neutron has much larger error but with the use of the cold NMR system [55] in combination with the multiple measurement techniques it is also possible to get down into the same uncertainty region as the proton.

### 3.6.4 Active Target Contributions

The figure of merit for this type of polarized target experiment is proportional to the active target contribution squared times polarization squared. The active target contribution is made of of the dilution factor and the packing fraction over the length of the target. The packing fraction can be determined using a method of cryogenic volume displacement measurement which compare an empty target cell to the full target cell used in the experiment. The target cell is filled with beads of solid  $\text{NH}_3$  material with a typical packing factor of about 60% with the rest of the space filled with liquid helium.

The dilution factor is the ratio of the number of polarizable nucleons to the total number of nucleons in the target material and can be defined as,

$$f = \frac{N_D \sigma_{D,H}}{N_N \sigma_N + N_D \sigma_D + \sum N_A \sigma_A}, \quad (24)$$

where  $N_D$  is the number of deuteron nuclei in the target and  $\sigma_D$  is the corresponding inclusive double differential scattering cross section,  $N_N$  is the nitrogen number of scattered nuclei with cross section  $\sigma_N$ , and  $N_A$  is the numbers of other scattering nuclei of mass number  $A$  with cross section  $\sigma_A$ . The denominator of the dilution factor can be written in terms of the relative volume ratio of  $\text{ND}_3$  to  $\text{LHe}$  in the target cell, the packing fraction  $p_f$ . For the case of a cylindrical target cell oriented along the magnetic field, the packing fraction is exactly equivalent to the percentage of the cell length filled with  $\text{NH}_3$  or  $\text{ND}_3$ . The dilution factor for  $\text{NH}_3$  is 0.176 and for  $\text{ND}_3$  is 0.3. The uncertainty in these factors from irreducible background is typically 2-3%.

## 3.7 Luminosity and Beam Intensity Uncertainty

### 3.7.1 Beam Profile

The typical profile of the beam delivered to the target is a two dimensional Gaussian with  $\sigma_x = 6.8$  mm,  $\sigma_y = 7.6$  mm. The beam will be clipped with collimators at  $\pm 1.25\sigma$ , giving a beam profile of  $\Delta x = 17$  mm,  $\Delta y = 19$  mm (see left plot in Fig. 19). The beam is expected to drift no more than  $\pm 2$  mm in the  $x$ -direction before collimation. The change of the luminosity of the beam due to the beam drifting is  $(N_{beam} - N_{drift})/N_{beam}$ . The right plot in Fig. 19 demonstrates that for a beam drift of  $x_{drift} = 2$  mm, the change in the delivered Luminosity is  $\Delta \mathcal{L} = 2.8\%$ .

### 3.7.2 Luminosity measurement

Several detector and measurement techniques are used in order to control systematic uncertainties from changing beam conditions, such as position, luminosity and shape. The absolute beam intensity will be determined by the Unser Monitors upstream of the target. The accuracy of Unser Monitors has been established to be 0.05% [58].

Four detectors at  $90^\circ$  to the beam (two horizontally and two vertically) will help monitor the instantaneous luminosity. Each of these detectors will consist of four plastic scintillators in coincidence and positioned outside of the shielding wall, pointing through a small hole in the shielding at the target. Fast MC simulations show that these detectors will detect  $\pi^\pm$ s,  $\mu^\pm$ s,  $\gamma$ s with  $E > 100$  MeV on the order of  $\sim 200$  kHz.

The ratio of every one of these detectors over the Unser Monitor measurement ( $N_{90^\circ}/N_{unser}$ ) will provide a fast relative luminosity measurement. If part of the beam profile deviates off the target after the Unser measurement (see example in Fig. 20), the  $90^\circ$  detectors will be able detect

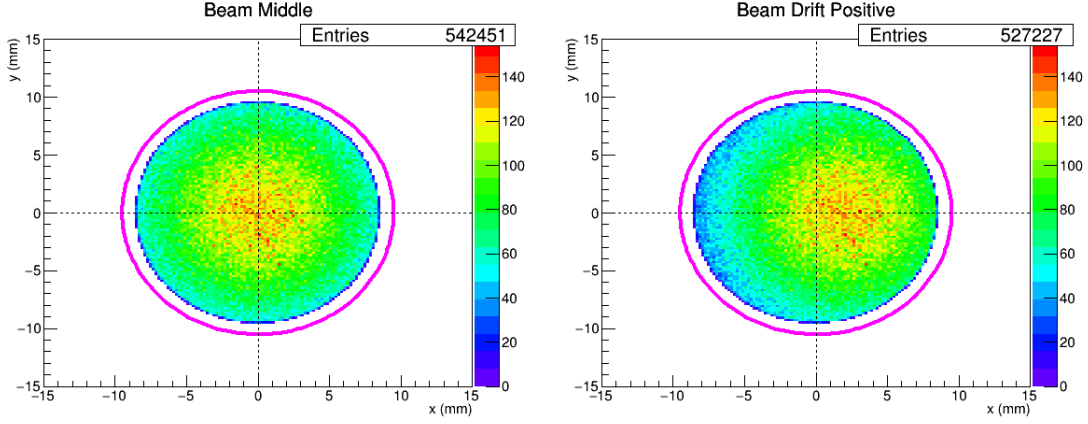


Figure 19: *Fast Monte-Carlo Plots demonstrating the beam drift before collimation. Magenta curve represents the Target Area. Left: Centered beam profile. Right: The beam is off center  $x = +2$  mm before collimation.*

luminosity changes to  $>1\%$ . This error comes from the systematic error on the four fold coincidence scintillators in each  $90^\circ$  detector, which we estimate to be  $\epsilon_{scint}^4 = 99 \pm 1\%$ .

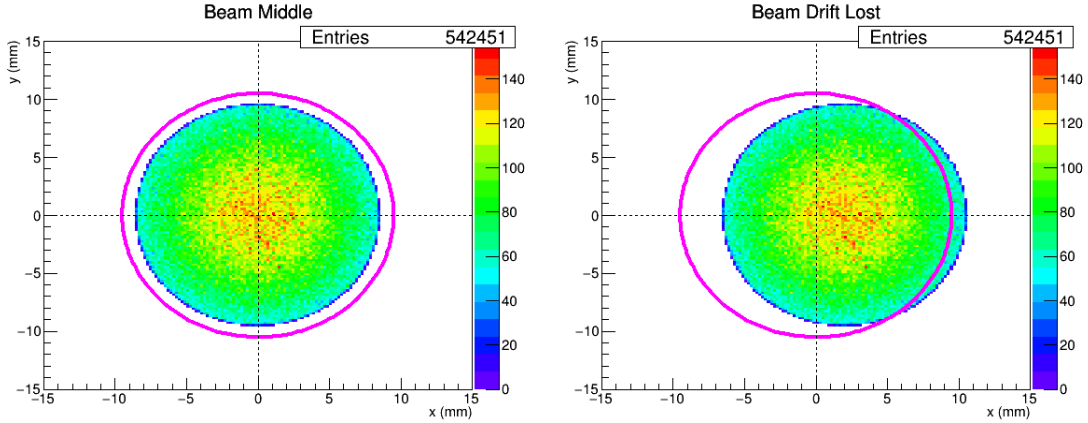


Figure 20: *Fast Monte-Carlo Plots demonstrating the beam drift. Magenta curve represents the Target Area. Left: Centered beam profile. Right: The beam is off center  $x = +2$  mm, such that part of the beam profile is not interacting with target.*

As an additional check on the relative beam intensity, a four plate RF cavity will be installed, which can also determine relative changes in the beam position,  $N_{90^\circ}/N_{RF} \propto (N_{90^\circ}/N_{unser})$ .

### 3.7.3 Consistency in Delivered Luminosity

Since extracting the Sivers asymmetry for the  $\bar{d}(x)$  requires measuring the ratio of  $\frac{\sigma^{pd}}{2\sigma^{pp}}$ , care has to be taken that the running conditions for both targets are as identical as possible. Our target system will have three identical cells, two filled with  $\text{NH}_3$  and the other with  $\text{ND}_3$ , or vice-versa. These will be interchanged on a regular basis to minimize systematic effects. The fourth position will have an empty cell for background subtraction, which can be replaced with a Carbon disk, to study false asymmetries.

### 3.8 Spectrometer Induced Uncertainties

A further source of systematic uncertainty may come from the muon spectrometer. Geometrical acceptance and effects on dimuon reconstruction due to temperature and pressure changes may have an effect on the measurement of the Drell-Yan  $A_N$ . To estimate the systematic uncertainty in the  $A_N$  measurement due to these changes in the spectrometer, the raw asymmetry of dimuons in the existing E906 data was used. A high statistics sample of the E906 data with stable running conditions was used for this study. An up-down spin direction was assigned randomly after a given length of data (e.g. one day), and the raw left-right asymmetry was calculated using the so called *square-root* formula.

$$\epsilon_{sqr}(\phi) = \frac{\sqrt{N^\uparrow(\phi) \cdot N^\downarrow(\phi + \pi)} - \sqrt{N^\downarrow(\phi) \cdot N^\uparrow(\phi + \pi)}}{\sqrt{N^\uparrow(\phi) \cdot N^\downarrow(\phi + \pi)} + \sqrt{N^\downarrow(\phi) \cdot N^\uparrow(\phi + \pi)}} \quad (25)$$

This process was repeated 5000 times. With random assignment of the spin direction, a Gaussian distribution centered around zero is expected. The RMS of the Gaussian should correspond to the statistical + systematic uncertainty due to the spectrometer,  $RMS^2 = \sigma_{stat}^2 + \sigma_{syst}^2$ . In order to estimate this error for the E1039 data, we need to take

$$\frac{\sigma_{E1039,syst}}{\sigma_{E1039,stat}} = \frac{\sigma_{syst}}{\sigma_{stat}} \quad (26)$$

$$\sigma_{E1039,syst} = \left( \frac{\sigma_{syst}}{\sigma_{stat}} \right) \times \sigma_{E1039,stat}, \quad (27)$$

so the absolute systematic error on the spectrometer will scale with the total statistical error.

The study was repeated five times, changing the length of data between spin assignments each time. An example of the Gaussian distribution for changing the spin direction once a day is shown in Fig. 21. The results are summarized in Table 5.

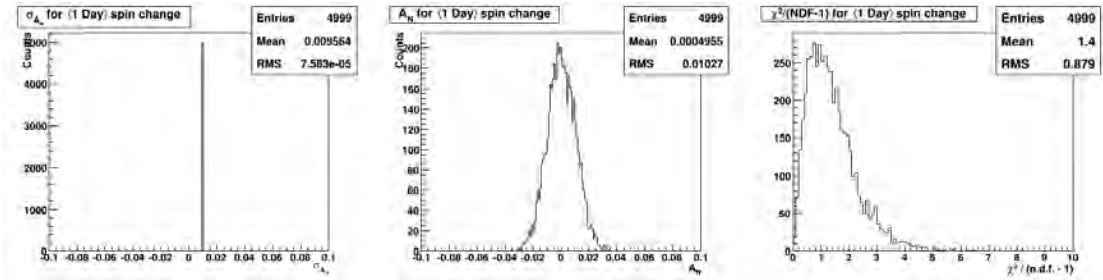


Figure 21: Plots describing the  $\epsilon_{sqr}$  of the E906 data where spin direction changes once a day. Left: The Mean value is the  $\sigma_{stat} = 0.95\%$  on  $\epsilon_{sqr}$ . Middle: The distribution of  $\epsilon_{sqr}$ , where  $RMS = \sqrt{\sigma_{stat}^2 + \sigma_{syst}^2} = 1.0\%$ . Right: The reduced  $\chi^2$  of each extracted  $A_N$  value.

A closer look at Table 5 indicates that if we carefully monitor the muon spectrometer and flip the polarization of the target every  $\sim 8$  hours, we expect to be able to minimize false asymmetries in  $A_N$  down to the  $10^{-3}$  level. As time increases between polarization flips, the systematic effect from drifts becomes clearly non-negligible. For 12-24 hours spin flips, if we have  $\sigma_{E1039,stat} \approx 3.0\%$  (see Table 4), we can expect an absolute systematic uncertainty of  $\sigma_{E1039,syst} \approx 1.0\%$ . Real running scenarios will require varying times between spin flips in order to keep a stable relative luminosity. For example, one can imagine a scenario where the spin is changed after 7 hours, but due to beam

Spin Change	$\sigma_{stat}$	RMS	$\sigma_{syst}$	$\sigma_{E1039,syst}$
<b>8 hours</b>	<b>0.95%</b>	<b>0.94%</b>	<b>&lt;0.10%</b>	<b>&lt;0.3%</b>
12 hours	0.95%	1.0%	0.31%	1.0%
24 hours	0.95%	1.0%	0.31%	1.0%
48 hours	0.96%	1.1%	0.53%	1.7%

Table 5: *The systematic error from the SeaQuest spectrometer on  $A_N$  vs time between spin changes. The 8 hour bold row represents the planned running scenario. The far right column gives the expected absolute systematic error on the measurement using Eq. 27, where  $\sigma_{E1039,stat} \approx 3.0\%$  from Table 4.*

conditions the next spin change is after 15 hours. Based on this likelihood, we estimate a worst case absolute systematic uncertainty due to the spectrometer to be  $\sigma_{E1039,syst} \leq 1.0\%$ . By keeping to a non-periodic schedule for target polarization change ( $8 \pm \sim 1$  hours) we can minimize systematic contributions from the diurnal cycle.

In conclusion, to ideally reduce possible long term systematic effects we plan to change the polarization of the target through change of the microwave frequency every 7-10 hours to avoid false asymmetry systematic effects on the measurement of  $A_N$ . In addition, we will change the field direction of the polarized target magnet as well as the direction of the field of the spectrometer. Combining measurements from different geometrical configurations with the same target cells and material will allow us to monitor for possible systematic drifts in the asymmetry due to effects on the muon spectrometer.

### 3.9 Overall Systematic Error

Table 6 lists estimates of the dominant contributions to the relative systematic error as described in the text.

Quantity	Error
Polarization Measurement	2.5%
Dilution Factor	2.5%
DAQ and Dead Time	1.5%
Relative Luminosity	1 %

Table 6: *Estimates for the relative systematic errors.*

Adding these numbers, we estimate our relative systematic error to be  $\leq 4\%$ . We also expect an absolute systematic error due to the muon spectrometer of  $\leq 1.0\%$ , as discussed in Sec. 3.8.

### 3.10 Expected Results

In Fig. 22 we show the expected results after two years of running with both  $\text{NH}_3$  and  $\text{ND}_3$  targets. The errors displayed are the statistical precision as listed in Table 4, while the expected systematic uncertainty is discussed in the caption. Also shown are two different theoretical predictions for the asymmetry by Sun and Yan [28] and Anselmino [59]. The calculations are based on global

fits to the available SIDIS data. The large discrepancy is a reflection of the fact that the current SIDIS data are insensitive to the seaquark contribution, thus leading to large uncertainties in the calculations. This is also reflected in the width of the uncertainty bands.

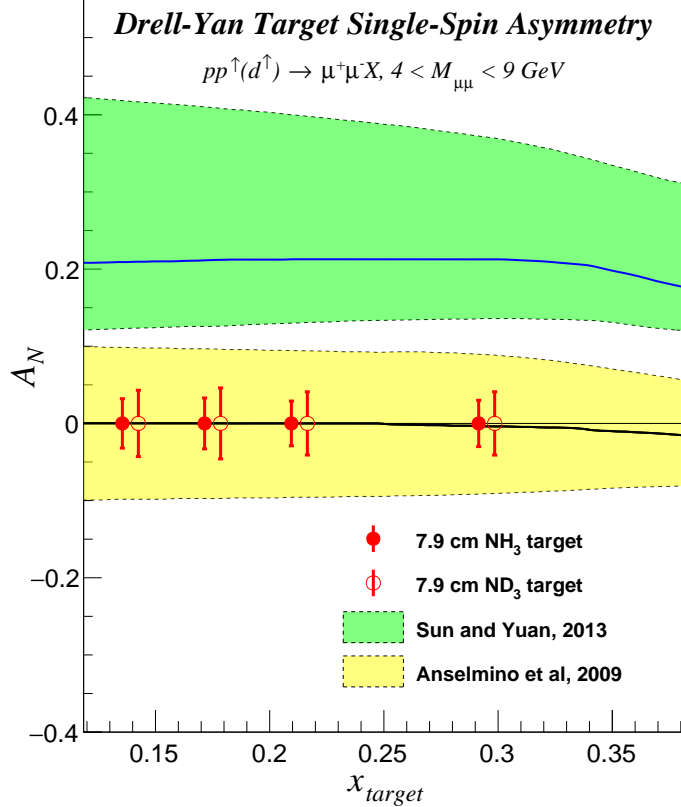


Figure 22: *Expected results after two years of combined running on NH<sub>3</sub> and ND<sub>3</sub> targets. The red error bars are statistical only. Absolute systematic uncertainty is estimated to be <1.0% (see Sec. 3.8), and the relative systematic uncertainty is 4.0%. The theory model predictions are for the NH<sub>3</sub> target only.*

## 4 Comparison to Competition

There have been plans for about a decade to perform a variety of experiments around the globe that aim to measure polarized Drell-Yan either with a polarized beam or a polarized target (see Table 7). COMPASS at CERN, SeaQuest at FNAL and Panda at GSI plan to perform fixed target experiments with either pion, proton or anti-proton beams, whereas PAX at GSI, NICA at JINR and fsPHENIX at BNL plan collider experiments with polarized proton beams. The fixed target experiments typically provide higher luminosity and the collider experiments tend to run at higher center of mass energy,  $s$ . NICA, fsPHENIX and SeaQuest will be sensitive to the interaction between valence quarks and sea antiquarks. PAX and COMPASS plan to measure the interaction between valence quarks and valence antiquarks, and are not sensitive to sea antiquarks. Panda is designed to study J/Ψ formation rather than Drell-Yan physics due to the low antiproton beam energy.

At present, only COMPASS has collected data using the 190 GeV  $\pi^-$  beam at CERN on a transversely polarized frozen ammonia ( $\text{NH}_3$ ) target. First results with limited statistics are expected in the fall of this year. But there are plans for a second year of polarized Drell-Yan studies in 2018 to measure the Siverts asymmetry  $A_N$  with a statistical precision  $\delta A_N$  of 0.014 (in a single  $x_F$ -bin centered at  $x_F = 0.2$ ). As shown in Table. 7, a polarized Drell-Yan experiment such as the SeaQuest experiment is needed, however, to measure the sign, the magnitude, and possibly the shape of the Siverts function with high precision.

experiment	particles	energy (GeV)	$x_b$ or $x_t$	rFOM	timeline
COMPASS (CERN)	$\pi^- + p^\uparrow$	190 $\sqrt{s} = 17.4$	$x_t = 0.1 - 0.3$	$1.1 \times 10^{-3}$	2015-2016 2018
PAX (GSI)	$p^\uparrow + \bar{p}$	collider $\sqrt{s} = 14$	$x_b = 0.1 - 0.9$	$2.3 \times 10^{-5}$	>2022?
PANDA (GSI)	$\bar{p} + p^\uparrow$	15 $\sqrt{s} = 5.5$	$x_t = 0.2 - 0.4$	$1.1 \times 10^{-4}$	>2020?
NICA (JINR)	$p^\uparrow + p$	collider $\sqrt{s} = 20$	$x_b = 0.1 - 0.8$	$6.8 \times 10^{-5}$	>2020
fsPHENIX (RHIC)	$p^\uparrow + p^\uparrow$	$\sqrt{s} = 200$ $\sqrt{s} = 510$	$x_b = 0.1 - 0.5$ $x_b = 0.05 - 0.6$	$4.0 \times 10^{-4}$ $2.1 \times 10^{-3}$	>2021
SeaQuest (unpol.) (FNAL E-906)	$p + p$	120 $\sqrt{s} = 15$	$x_t = 0.1 - 0.45$ $x_b = 0.35 - 0.85$	--	2012-2017
pol tgt DY (FNAL E-1039)	$p + p^\uparrow$	120 $\sqrt{s} = 15$	$x_t = 0.1 - 0.5$	0.09	>2018
pol beam DY (FNAL E-1027)	$p^\uparrow + p$	120 $\sqrt{s} = 15$	$x_b = 0.35 - 0.85$	1	>2020

Table 7: *A summary of polarized and unpolarized Drell-Yan experiments at various laboratories around the world. Note that  $x_b$  and  $x_t$  are the parton momentum fractions in the beam and target, respectively. The relative figure of merit (rFOM) is the luminosity times beam or target polarization squared times the dilution factor squared, relative to E-1027.*

The big attraction for a polarized Drell-Yan program at the Fermilab Main Injector is the very high luminosity and the large  $x$ -coverage afforded by a primary beam and a fixed target. This is demonstrated in Table 7, column 'rFOM' which shows that running an experiment with a secondary beam, such as the  $\pi^-$  beam at COMPASS, or running in collider mode, such as at fsPHENIX, will result in a relative figure of merit that is about a factor of 100 – 1,000 smaller than using a primary beam on a fixed target. The SeaQuest spectrometer accommodates a large coverage in parton momentum fraction  $x$ , *i.e.*  $x_b = 0.35 - 0.85$  covering the valence quark region, and  $x_t = 0.1 - 0.5$  covering the sea quark region. This allows us to perform the first sea-quark Siverts asymmetry measurement and determine the sign and magnitude of the  $\bar{u}$  and  $\bar{d}$  Siverts distributions, using the polarized hydrogen target. If the measured asymmetry is non-zero, it would be a major discovery, and be a “smoking gun” evidence for the orbital angular momentum of the  $\bar{u}$  quark being non-zero.

## 5 Budget Discussion

In the following we will describe some of the major cost expenditures of experiment E1039 and the current estimates.

## 5.1 Liquefier System and Pump Installation

The major cryogenic issues with a polarized  $^4\text{He}$  target are the liquid He consumption and the collection of the exhaust gas. Keeping the target at 1K while irradiating it with the microwave requires evaporation of 100 liters of liquid He per day through pumping. Not recovering the Helium gas after the ROOTS pumps would lead to wasting an unacceptable amount of a nonrenewable resource at a cost of \$600,000 for two years of running. New DOE guidelines require us to install a closed loop Helium liquefier system. Furthermore, such a system needs special plumbing and recovery infrastructure consisting of Helium and Nitrogen transfer lines, pumping lines from the target to the ROOTS pumps as well as a special quenchline, which would handle the Helium exhaust gas in case of a magnet quench. We have identified two Linde L1410 liquefiers (one at FNAL and one at the University of Illinois), which we could have refurbished as part of a whole package. Quantum Technology (QT), in 2015, has provided us with a preliminary bid for a closed loop system, including rebuilding one of these liquefiers for \$408,000. This quote assumed a cost of \$30,000 for refurbishing these L1410s. However, a firm estimate for this can only be provided when the liquefier is at Quantum Technoloy and evaluated for the work needed (see quote in Appendix). In an independent, oral communication from Linde industries (the original manufacturer), the cost for rebuilding was quoted to us as up to \$250,000. We have decided to use this higher estimate together with the closed loop system quote from Quantum Technology (removing the refurbishing amount from the QT quote) to estimate the total liquefier costs at \$628,000.

The costs for the Helium and Nitrogen transfer lines is contingent on the final design and installation of the cryo system. While we have a preliminary design, this will need further detailed studies in collaboration with FNAL ES&H personnel. The estimate for the liquid Helium and Nitrogen transfer lines, based on the current design, is \$50,000. The estimate for the Helium pump lines is \$20,000. The liquefier and the pump lines need two new dedicated 200A electrical circuits to be installed as well as switches on the two magnets to flip the sign of the magnetic fields, at a cost of \$25,000.

## 5.2 Beam Line Changes

As described above, the modifications to the beamline will require the installation of two collimators in NM2 to shape the beam, as well as a collimator in NM3 to shield the superconducting coils of the target magnet. The current cost estimate for this is roughly \$330,000, which is mainly labor.

## 5.3 Shielding and Target Cave Modifications

This cost can only be estimated once the final design of the shielding has been performed and the scope of the necessary work been determined. This will require close collaboration between ES&H, Accelerator and Physics divisions at FNAL with LANL engineering. The main cost of this will be labor for stacking the E1039 shielding. The FNAL estimate for completely unstacking (which is more than we would need) the SeaQuest shielding is \$40,000. After the removal of the E906 shielding the work on the new shielding configuration can commence. The FNAL provided labor cost estimate for this work is \$300,000.

As described in the section on Integration, the target cave area has to be modified to allow for the additional height required to change the target stick, as well as accomodating the move of the target further upstream. The FNAL provided estimate for this is \$180,000 with \$170,000 in labor. This will include the costs for installing the transfer lines.

## 5.4 Total Installation Costs

In the following we summarize the major costs associated with mounting the E1039 experiment at Fermilab. We have split up the costs into equipment and labor needs as outlined. The costs are based on quotes from vendors, previous purchases and estimates provided by FNAL personnel. The contingencies for items with quotes have been lowered, however in the case of Quantum Technology, we have increased the costs of the liquefier to reflect the higher oral quote from Linde. Based on our detailed knowledge of work necessary to remove the E906 shielding, we felt confident to lower this contingency to 10%.

Item	Equipment	Labor	Source of estimate	Contingency	Costs
Close Loop Liquefier	\$628,000		Quote	10 %	\$691,000
Transfer Lines	\$50 000		Prev Purchases	20 %	\$60,000
Pump Lines	\$20,000		Quote	10 %	\$22,000
Electrical Installations	\$5,000	\$20,000	FNAL	25 %	\$32,000
Beam Line	\$10,000	\$320,000	FNAL	25 %	\$413,000
E906 shielding		\$40,000	FNAL	10 %	\$44,000
E1039 shielding		\$300,000	FNAL	20 %	\$360,000
Target Cave	\$10,000	\$170,000	FNAL	20 %	\$216,000
<b>Total</b>	<b>\$723,000</b>	<b>\$850,000</b>			<b>\$ 1,838,000</b>

Table 8: *Total Budget Estimates for E1039*

We are asking for support from the DOE Office of Nuclear Physics to mount and operate experiment E1039 at Fermilab. We expect that FNAL will cover some of these costs, but this has to be negotiated between DOE NP, DOE HP and FNAL.

# Appendices

## A Fermilab PAC 2013 and 2015 reviews

In 2013 the measurement of the Sivers asymmetry was presented to the FNAL Program Advisory Committee (PAC) as a letter of intent (P-1027), which can be found in the appendix D. Even though we submitted this as a LOI, the PAC recommended stage-1 approval, a testimony to the quality of the physics. At Fermilab, the PAC can only approve stage-1, while stage-2 is granted by the director, once the funding for the experiment has been secured. In the following we quote the relevant section from the 2013 PAC report [62]:

*Drell-Yan Experiment with a Polarized Proton Target (P-1039) Members of the SeaQuest Collaboration presented a proposal (P-1039) for a new Drell-Yan experiment at Fermilab. P-1039 proposes to perform the first measurement of the Sivers function of sea anti-quarks by adding a new LANL-designed polarized proton target to the existing E906 detector. No major changes are required to the beam line. The physics addressed by P-1039 is similar to that addressed by P-1027, a proposal presented to the PAC in 2012. Both propose to perform measurements aiming to resolve the proton spin puzzle, a topic that is important to the nuclear physics community and*

is of interest to the high-energy physics community as well. While P-1027 aims to measure the Sivers function for valence quarks, P-1039 proposes to perform the same measurement on sea anti-quarks. Since there are indications from other experiments that the Sivers function for valence quarks is small, the measurement proposed by P-1039 is more promising in terms of providing a possible solution to the proton spin puzzle. By using a polarized target instead of a polarized beam, P-1039 would address this interesting physics topic while keeping to a minimum the impact on the Fermilab accelerator division and the rest of the Fermilab physics program. This is not the case for P-1027, which requires significant resources to develop a polarized beam and which more severely disrupts the beam to NOvA. The PAC also appreciates the opportunity offered by this proposal to continue the partnership between Fermilab and the nuclear physics community. Given the pressure on the accelerator division and the overriding responsibility of the Lab to support its core neutrino program, the PAC recommends that priority should be given to P-1039 over P-1027, and hence recommends Stage-1 approval for P-1039, contingent on the funding from DOE Office of Nuclear Physics (NP) for the project and continued minimal impact on the high-priority core program. Because of the significantly smaller impact of P-1039 on the Fermilab infrastructure, NP funding could be easier to obtain and the experiment could start earlier.

In January 2015 we presented an update to the PAC on the status of the preparation for the experiment, where again the PAC expressed their support for this effort [63]:

**LOI: P-1039 UPDATE: Drell-Yan Experiment with Polarized Target (SeaQuest extension)** *The SeaQuest extension E-1039 aims at resolving the proton spin puzzle, and in particular measuring the Sivers function for sea quarks. E-1039 is planned to achieve a sensitivity level far superior to other experiments. The collaboration presented a very detailed and very well thought out plan for the transition from SeaQuest to E-1039. **The case was successfully made that unique measurements could be made by E-1039 to complement those from experiments at other facilities, notably COMPASS at CERN** (bold added for emphasis). The PAC appreciates the opportunity offered by this proposal to continue the partnership between Fermilab and the nuclear physics community. We encourage the development of a TSW in preparation for Stage 2 approval, which will require an expectation of full funding from the DOE Office of Nuclear Physics.*

## B The current accomplishments from the LDRD

In 2013 LANL has awarded an internal grant jointly to Physics and Theory divisions to build a polarized target and provide theoretical guidance for this experiment. This grant has provided 5 M\$ for labor and equipment over three years.

### B.1 Experimental

This internal grant allowed LANL and UVa to convert an old, longitudinally polarized target into a transverse one and refurbish the refrigerator shown in Fig. 16. In addition, LANL's funds have been used to buy the necessary additional equipment, like the ROOTS pump system, microwave tube and power supply and develop a new NMR system to measure the polarization. This system is based on the Liverpool Q-meter design [61], but with new components, which allow a much more compact system. The new NMR is VME based and one crate will house the electronics for

all nine NMR coils in use in our target system (3 cells per stick). This new system is shown in Fig 23



Figure 23: *The new LANL VME based NMR readout.*

In April 2016, the polarized target system was tested with a small microwave horn and one NMR coil. In this test the irradiated volume by the horn was smaller than the volume covered by the NMR system, leading to a reduced polarization signal. We estimate that this mismatch results in a  $\sim 20\%$  smaller measured polarization. Even with this system we measured a polarization of 72% as show in Figure 24. With the new microwave horn and three NMR coils, we are confident of reaching a maximum polarization in excess of 95%.

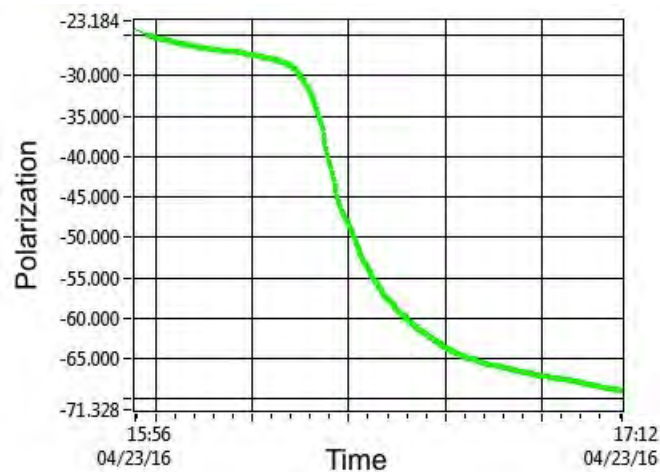


Figure 24: *The first polarization measurement with the new E1039 target.*

To summarize, LANL's investment has allowed us to build the world's highest luminosity transversely polarized target.

## B.2 Theoretical

Extracting the spin structure of the nucleon from the measurements of the quark Sivers asymmetry requires self-consistent and detailed theoretical interpretation of the results from Drell-Yan experiment and from semi-inclusive deep inelastic lepton-proton scattering. The LDRD DR grant allowed us to initiate an integrated theory effort with three complementary components – perturbative QCD calculations, Soft Collinear Effective theory, and lattice gauge QCD. The ultimate goal is a much-improved description of the dynamic internal landscape of the nucleon from measurements of the Sivers asymmetry. The perturbative QCD effort has resulted in next-to-leading order calculations of the Sivers asymmetry in SIDIS and Drell-Yan and an extraction of the Sivers function with next-to-leading logarithmic accuracy. Model calculations of quasi-parton distribution functions were also performed. The Soft Collinear Effective Theory effort has demonstrated the equivalence of the pQCD and SCET resummation approaches and calculated two-loop soft functions for use in a variety of processes. Lattice QCD has produced new results for the moments of the Sivers asymmetry from connected diagrams and compared to results from global fitting. A new method for the evaluation of disconnected diagrams has also been investigated. The integrated theory model, with its pQCD, SCET and LQCD components, was the stepping stone for the formation of the TMD Topical Collaboration in nuclear theory.

## B.3 LANL reviews

During the course of the LDRD project the LDRD office required two reviews of the physics, technical efforts and progress both in the experimental as well as the theoretical aspects of the LDRD project. The review panels included external as well as internal members of the community. The first review committee was composed of: C. Keith, Jefferson Lab, S. Kuhn, Old Dominion University and J. Qiu, Brookhaven National Laboratory as external members and C. Olinger, M. Brooks and B. Louis from LANL as internal. The second committee consisted of G. Dodge, Old Dominion University, and L. Gamberg, Penn State University as well as A. Hayes-Sterbenz and M. Brooks from LANL. In both reviews the physics program as well as the experimental and theoretical have been consistently been deemed as outstanding. In the following we show excerpts from the two reviews:

Review Jan 2015

**Quality : Outstanding** *The quark and gluon Sivers functions of a polarized proton describe the quantum correlations between its spin and the direction as well as the strength of confined orbital motion of quarks and gluons within it. They encode critical information on the confined structure and motion of quarks and gluons making up the proton's properties, such as the spin, and are fundamental properties of QCD dynamics. The predicted sign change of the Sivers functions measured in Semi-inclusive DIS to that measured in Drell-Yan processes is deeply rooted in the gauge property of QCD and the validity of QCD factorization. Owing to the color confinement - the defining property of QCD, meaning that we can't probe the proton's partonic structure without QCD factorization - developing the formalism to precisely connect the QCD dynamics to the measured cross sections of leptons and hadrons is an area of active research. The predicted sign change of Sivers functions has been recognized as the most important test of and challenge to our understanding of QCD dynamics. It attracted tremendous theoretical and experimental effort worldwide to find a way to confirm or disapprove this prediction. The Sivers functions have been*

extracted from Semi-inclusive DIS experiments, but they have not been extracted from any Drell-Yan experiment yet. Along with the proton-proton Drell-Yan experiment of this DR at Fermilab, the COMPASS experiment at CERN is pursuing Drell-Yan measurement in pion-proton collisions, while the RHIC Spin program at Brookhaven National Lab is trying to extract the Sivers functions from its Drell-Yan like  $W$ -physics program. All three experiments worldwide are critically important and complementary to each other due to the difference in beams and energy scales where the Sivers functions are probed. The proposed measurement of Sivers functions for anti-quarks by this DR cannot be replaced by any currently proposed experiments, and will lead to a fundamental advance of our knowledge in hadron physics and QCD dynamics far beyond the more than thirty-year effort in extracting the parton distribution functions.

Review Jan 2016

**Overall Grade: Outstanding** *The emerging picture of the nucleon in its three dimensional (3-D longitudinal and transverse) momentum structure is that it is a dynamical system of confined quarks and gluons with the dynamics governed by the gauge symmetry of Quantum Chromodynamics (QCD). Polarizing the nucleon sets up a laboratory to probe and study the essential quantum correlations that emerge from the QCD description of between the spin and the direction as well as the strength of confined orbital motion of quarks and gluons within the nucleon. The Sivers function describes critical information on these correlations. Owing to the color confinement - the defining property of QCD, meaning that we can't probe the proton's partonic structure without the tools of QCD factorization - developing the formalism to precisely connect the QCD dynamics to the measured cross sections of leptons and hadrons is an area of active research. The predicted sign change of the Sivers functions measured in semi-inclusive DIS to that measured in Drell-Yan processes is reflected in the gauge property of QCD and the validity of QCD factorization. This DR has focused on the theory and measurement of the Sivers function to study the nucleon from the fundamental theory of quark and gluon interactions. The goal of understanding the spin of the proton remains one of the key scientific questions in nuclear physics today and was discussed in the 2015 Long Range Plan for Nuclear Science. In order to make progress on this longstanding issue, it is crucial to look for signatures of quark orbital motion in the proton. One of the few ways to do that is to measure the Drell-Yan process with a polarized proton target and proton beam as proposed for Fermilab in E1039. By accessing the Sivers asymmetry primarily of the anti quarks in the proton, E1039 provides a unique and critical contribution to our understanding of the structure of the nucleon. The measurement remains as important today as it was a year ago, and the high luminosity polarized target that the LDRD team has built is absolutely critical to the success of that project. The technical challenges of adapting the polarized target to the needs of the Fermilab experiment are many, but the LDRD team has succeeded, thus providing the community with a new way to study quark orbital motion in the proton.*

## C Future Physics Opportunities

### C.1 Deuteron Tensor Function $b_1$

Additional insight into the angular momentum comes from the study of the tensor structure function  $b_1$  of spin-1 hadrons, in our case the deuteron. Such a tensor contribution has to identically

vanish if the proton and the nucleon are in a simple relative S state. For a spin-1 system in a magnetic field along the z-axis, the Zeeman effect leads to three sublevels  $I_z = +1, 0, -1$  with populations  $p_+$ ,  $p_0$  and  $p_-$  respectively. Contrary to the spin  $\frac{1}{2}$  system where we have only the vector polarization  $P_z = (p_+ - p_-)$ , in the case of spin 1 we also have a tensor polarization  $P_{zz} = (p_+ - p_0) - (p_0 - p_-) = 1 - 3p_0$  (since  $p_+ + p_0 + p_- = 1$ ).

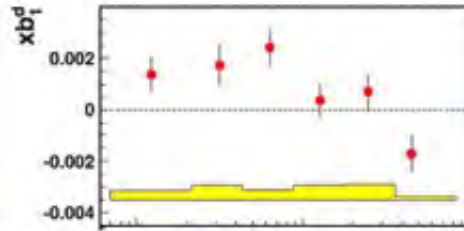
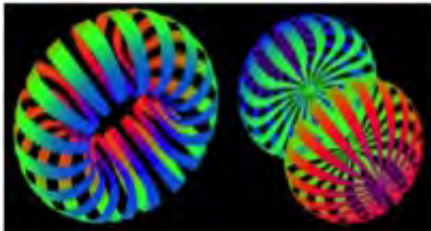


Figure 25: *The  $m = 0$  (left) and  $m = 1$  state (right) of the deuteron*      Figure 26: *The HERMES measurements of  $b_1$*

The maximum tensor value of  $P_{zz} = -2$  is reached, when the  $m = \pm 1$  states are vanishing, and the surface of constant density has a toroidal shape, as shown in the left picture of Fig. 25. The figure on the right represents the same quantity for a system where the vector polarization is maximized ( $m = \pm 1$ ). This additional tensor polarization state now leads to tensor structure functions  $b_1$ ,  $b_2$ ,  $b_3$  and  $b_4$ , where in the parton model  $b_1$  expresses the difference between the partonic constituency in a  $|m| = 1$  target and an  $|m| = 0$  target. This is an extremely interesting result, since it means that  $b_1$  not only depends on the quark distributions (a property of the nucleon) but also on the spin state of the two nucleons in the nucleus (a nuclear property), thus forming a bridge between nucleon and nuclear physics. While all available models today predict a small to vanishing value of  $b_1$ , data from HERMES [64] indicate that this value is non-zero and has a cross over point at  $x = 0.3$  as shown in Fig. 26. Given the large acceptance of our spectrometer, we are ideally suited to see this cross over.

## C.2 Explore gluon TMD/Twist-3 trigluon correlation functions and QCD dynamics with heavy quarks

Apart from the sea-quark Sivers function measurements, E1039 also provides a unique opportunity to study the poorly known gluon Sivers/Twist-3 correlation functions at a very interesting kinematic region of  $0.1 < x_T < 0.2$  using heavy quarks. Large TSSAs up to  $\simeq 40\%$  have been observed in light hadron production at various collision energies in the forward  $x_F$  region, corresponding to a momentum fraction  $0.1 < x_B < 0.5$  of the incoming transversely polarized proton. The observed large asymmetries are normally attributed to the valence quark Sivers and/or Collins effects (or corresponding twist-3 correlation functions in the collinear factorization framework) in both polarized SIDIS and p+p collisions, since the production process is dominated by the interaction of the incoming valence quarks with partons from the polarized target. The valence quark Sivers and Collins functions have been well measured at the HERMES, COMPASS and JLab experiments.

However, due to experimental limitations, very little data are available to directly constrain the gluon Sivers function in this large-x region. It is also important to note that there are plenty of gluons inside the proton, comparable even to valence quarks, as seen in Figure 7. Therefore it is necessary to study the gluon Sivers function in order to complete our understanding of quark and gluon TMD distributions inside the polarized proton.

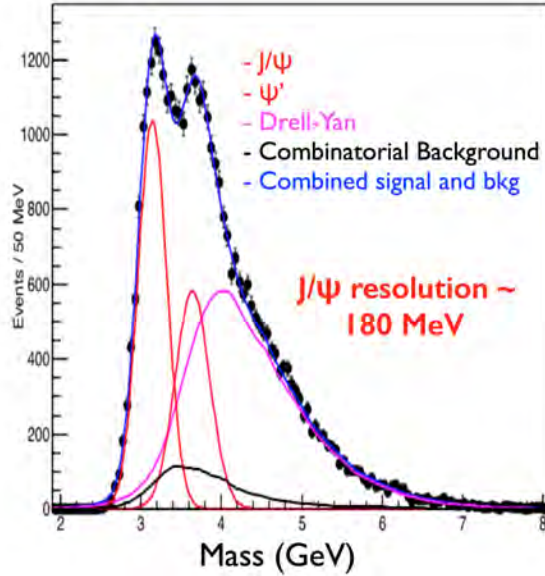


Figure 27: *Dimuon mass distribution from E906. Note the significant number of  $J/\Psi$  events collected (peak at 3.1 GeV), event though they were highly suppressed by E906 dimuon trigger due to DAQ limitations. With the DAQ upgrade, up to one million  $J/\Psi$  can be recorded in E1039.*

It is expected that charmonia such as the  $J/\Psi$  are predominantly produced via gluon-gluon interactions at the E1039 center of mass energy. Thus the heavy flavor transverse single spin asymmetry is sensitive to the gluon Sivers functions (or tri-gluon correlation functions in the collinear framework). In particular the  $J/\Psi$  TSSA can be used to study gluon Sivers functions and also QCD dynamics in hadron production. Figure 27 shows the dimuon invariant mass distribution from E906 experiment. Copious  $J/\Psi$  events are collected in E906 and we expect an improved acceptance for  $J/\Psi$  in E1039.

Recently, the PHENIX experiment at the Relativistic Heavy Ion Collider at Brookhaven National Laboratory has published the first measurement of the  $J/\Psi$  TSSA to study the gluon Sivers function. However, the data are too statistically limited to draw a strong conclusion. With much improved statistics from E1039, we expect an order of magnitude statistical improvement over the PHENIX results, which will shed new light on our understanding of gluon Sivers function and heavy flavor TSSA. Figure 28 shows the expected statistical uncertainties for the  $J/\Psi$  TSSA as a function of  $x_T$  from E1039.

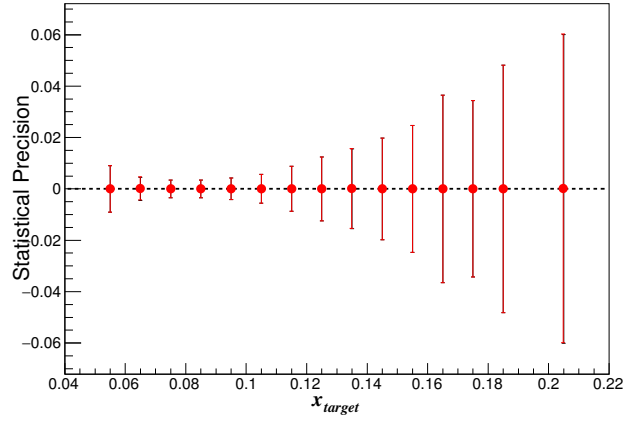


Figure 28: *Expected statistical uncertainties for  $J/\Psi$  TSSA from E1039.*

## D Letter of Intent P-1039

## Letter of Intent for a Drell-Yan experiment with a polarized proton target

Co-Spokespersons: **A. Klein, X. Jiang**, Los Alamos National Laboratory

### List of Collaborators:

D. Geesaman, P. Reimer  
*Argonne National Laboratory, Argonne, IL 60439*

C. Brown, D. Christian  
*Fermi National Accelerator Laboratory, Batavia IL 60510*

M. Dieffenhaller, J.-C. Peng  
*University of Illinois, Urbana, IL 61081*

W.-C. Chang, Y.-C. Chen  
*Institute of Physics, Academia Sinica, Taiwan*

S. Sawada  
*KEK, Tsukuba, Ibaraki 305-0801, Japan*

T.-H. Chang  
*Ling-Tung University, Taiwan*

J. Huang, X. Jiang, M. Leitch, A. Klein, K. Liu, M. Liu, P. McGaughy  
*Los Alamos National Laboratory, Los Alamos, NM 87545*

E. Beise, K. Nakahara  
*University of Maryland, College Park, MD 20742*

C. Aidala, W. Lorenzon, R. Raymond  
*University of Michigan, Ann Arbor, MI 48109-1040*

T. Badman, E. Long, K. Sliker, R. Zielinski  
*University of New Hampshire, Durham, NH 03824*

R.-S. Guo  
*National Kaohsiung Normal University, Taiwan*

Y. Goto  
*RIKEN, Wako, Saitama 351-01, Japan*

L. El Fassi, K. Myers, R. Ransome, A. Tadealli, B. Tice  
*Rutgers University, Rutgers NJ 08544*

J.-P. Chen  
*Thomas Jefferson National Accelerator Facility, Newport News, VA 23606*

K. Nakano, T.-A. Shibata  
*Tokyo Institute of Technology, Tokyo 152-8551, Japan*

D. Crabb, D. Day, D. Keller, O. Rondon  
*University of Virginia, Charlottesville, VA 22904*

### 1. Physics motivation

It is well known that the proton is a spin-1/2 particle, but how the constituents (quarks and gluons) assemble to this quantized spin is still a mystery. There is a worldwide effort to map out the individual contributions to the proton spin [1,2]. It is established that the quark spins contribute around 30%, while the gluon intrinsic angular momentum is still under active investigation at the Relativistic Heavy Ion Collider [3]. Fully resolving the proton spin puzzle requires information on the orbital angular momentum (OAM) of both quarks and gluons. Recent studies have shown that the so-called transverse momentum dependent parton distribution functions (TMDs) can inform us about the OAM of the partons.

One of the most important TMDs, and the main focus of this LOI, is the so-called Sivers function [4]. It was introduced in 1990 to help explain the large transverse single-spin asymmetries observed in hadronic pion production at Fermilab [5]. The quark Sivers function represents the momentum distribution of unpolarized quarks inside a transversely polarized proton, through a correlation between the quark momentum transverse to the beam and the proton spin. On one hand, the Sivers function contains information on both the longitudinal and transverse motion of the partons and provides a unique way to perform 3-dimensional proton tomography in momentum space [1, 2]. On the other hand, it has been shown that there is a close connection between the Sivers function and quark OAM. Though the search for a rigorous, model-independent connection is still ongoing, it is clear that the existence of a non-zero Sivers function requires non-zero quark OAM [1]. From a detailed analysis of the azimuthal distribution of the produced particles from a transversely polarized nucleon, one can deduce properties of the nucleon structure.

This approach has been used in Semi-Inclusive Deep Inelastic Scattering (SIDIS) experiments, where non-zero values of the Sivers function from HERMES [6], COMPASS [7] and JLab [8] have indicated that the orbital angular momentum of the up quarks is positive ( $L_{u_v} > 0$ ) but of the down quarks is negative ( $L_{d_v} < 0$ ). The anti-down versus anti-up quark excess in the proton observed in Drell-Yan (DY) measurements by E866 [Figure 1], when interpreted in the pion cloud model, provides a strong hint that the sea quarks contribute significantly to the orbital angular momentum [9], in the x range where significant valence quark Sivers asymmetries were observed in SIDIS. However, current SIDIS experiments have little sensitivity to the antiquark Sivers asymmetry in this kinematic range. Thus, a direct measurement of the Sivers function for the antiquarks has become crucial and can only be accessed cleanly via the Drell-Yan process. We propose to carry out the first measurement of the sea quark Sivers function, using Drell-Yan production from an unpolarized 120 GeV proton beam scattering off a transversely polarized proton target.

Besides helping to resolve the proton spin puzzle, this proposal helps address the recent NSAC milestone HP13 to “test unique QCD predictions for relations between single transverse spin phenomena in p-p scattering and those observed in deep inelastic lepton scattering.” A fundamental prediction of QCD is that the Sivers function changes sign when going from SIDIS to DY production [10]. This prediction is deeply rooted in the gauge structure of QCD as a field theory, and is based on the well-known QCD factorization formalism widely used in interpreting high-energy experimental data. Thus, its experimental verification or refutation is crucial. The

existing SIDIS data from HERMES, COMPASS and Jlab [6, 7, 8] have enabled us only to extract the Sivers function of valence quarks. This LOI proposes to make the first determination of the size and the sign of the sea quark Sivers function. Combined with higher luminosity SIDIS experiments planned at JLAB, which aim to measure the Sivers distribution for sea quarks, our results would allow a test of this fundamental prediction of QCD. Higher luminosity SIDIS experiments planned at JLAB should be able to measure the sea quark Sivers distribution for direct comparison with our results.

To summarize, we propose to make the first measurement of the Sivers function of sea quarks, which is expected to be non-zero if the sea quarks contribute orbital angular momentum to the proton spin, as expected from the pion cloud model which also partially explains the E866 results. Thus, we will be able to deduce whether or not sea quark orbital motion contributes significantly to the proton spin. Specifically, we will determine the contribution from the anti-up quarks, with Bjorken- $x$  in the range of  $\sim 0.1$  to  $0.5$ . Drell-Yan production off a polarized proton target has never been measured and is complementary to the recently approved (stage-1) experiment E1027 at Fermilab [11], which will measure the Sivers function of the valence quarks using a polarized proton beam on an unpolarized proton target. If the measured sea quark Sivers function is non-zero, we will also determine its sign.

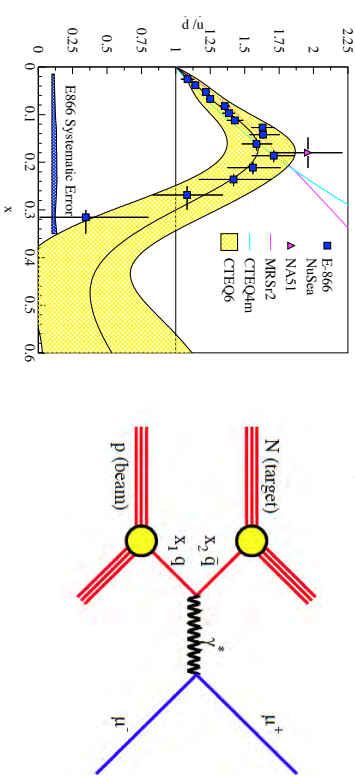


Figure 1. E866 DY result for anti-down versus anti-up quark content of the proton (left). If the excess of anti-down quarks is due to a pion cloud around the proton, then the pions (and sea quarks) contribute a significant amount of orbital angular momentum. On the right is a Feynman diagram for the Drell-Yan process.

On the theoretical side, Gupta, Kang, View and collaborators are currently developing numerical simulation packages at LANL to provide accurate QCD predictions for the DY single-spin asymmetry in the kinematic region relevant to our experiment. Once our DY data become available, they will use a global fitting procedure to extract the sign and the shape of the Sivers function. To test the predicted sign change between SIDIS and DY, sea quark SIDIS data will also be required. In addition, they are performing a Lattice QCD calculation of the Sivers function to also pinpoint the sign in these two processes and to estimate the magnitude.

In order to perform the proposed measurement, a new LANL-designed high-luminosity polarized proton target system needs to be added to the existing E906 dimuon spectrometer at Fermilab (Figure 2). An essential component of this system is a superconducting magnet that produces a uniform field transverse to the beam direction. LANL, University of Virginia (UVA) and Oxford Instruments are refurbishing an existing 5 Tesla (T) superconducting magnet that will provide the necessary holding field for a polarized ammonia (NH<sub>3</sub>) target. In addition, we need to build a new refrigerator and microwave system to populate the polarized spin states. The existing E906 cryogenic targets will be replaced with this polarized ammonia target. In section 4, we further discuss the required modifications to the E906 experiment.

We wish to emphasize that our proposed measurement is complementary to E1027. E1027 will measure the asymmetry and the crucial determination of the sign change for valence quarks. Our data will determine the sign and magnitude of the sea quark asymmetry. Furthermore, in semi-inclusive deep-inelastic scattering (SIDIS) measurements, there is, at leading twist, one structure function per TMD. In Drell-Yan measurements, there are at least two structure functions per TMD [12]. A Drell-Yan experiment with both a polarized beam and a polarized target would provide unique access to these structure functions. Therefore, it is imperative to perform both experiments. Similarly, our experiment is complementary to the COMPASS experiment at CERN [13], which concentrates on valence quarks.

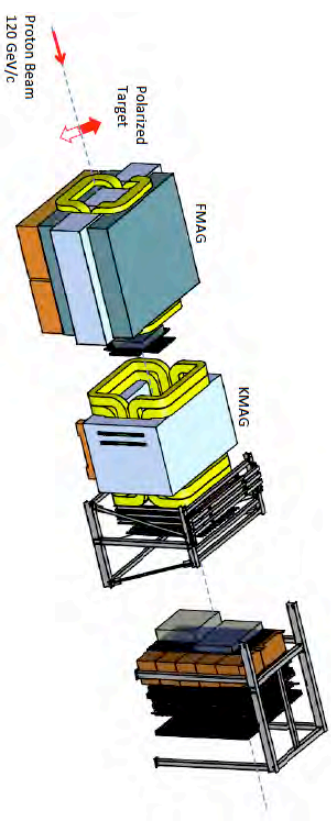


Figure 2. E906 spectrometer, showing the two dipole magnets, tracking stations and muon identifier. Shown on the left is the vertical direction of the polarization of the ammonia target. Further details of the target are shown in Figure 3.

## 2. Proposed measurement and experimental facility

The E906 spectrometer was designed to perform Drell-Yan measurements covering  $x_2$  from 0.1 to 0.5. This is an excellent kinematic range for the proposed sea quark Sivers function measurement, covering the region of large anti-down quark excess observed by E866, where large pion-cloud effects may be expected. The contributions from target valence quarks at large  $x_2$  can be made small by choosing  $x_F > 0$ . The existing 120 GeV Main Injector beam line and beam intensity of  $10^{13}$  protons per 5 second spill, once a minute, are also appropriate. Some

improvements to the final beam focus, beam position and halo monitoring may be required to minimize the size of the beam spot and avoid quenching the superconducting target magnet. Accurate relative beam luminosity measurements are also needed to minimize systematic uncertainties due to false asymmetries.

A 5 T superconducting magnet from LANL has recently been re-commissioned at full field at UVA during February, 2013. This target magnet was originally designed for longitudinal polarization (relative to the beam) while our experiment requires transverse polarization. Oxford Instruments of England will rotate the magnet coils to the transverse direction and reconnect the cryogenic supply lines. LANL and UVA will be jointly responsible for the polarized target. We will design and construct a target ladder insert, microwave and NMR systems. Furthermore, we will provide the necessary helium pumping system to reach 1 K, and irradiate the  $\text{NH}_3$  beads at NIST. We emphasize that this is all proven technology and is almost identical to an existing polarized  $\text{NH}_3$  target that has been successfully operated for years at SLAC and Jefferson Lab.

The target is polarized using Dynamic Nuclear Polarization (DNP) and is shown schematically in Figure 3. The beam direction is into the page, so that the target polarization is transverse to the beam direction. The existing superconducting magnet is also shown in the figure.

While the magnetic moment of the proton is too small to lead to a sizable polarization in a 5 T field through the Zeeman effect, electrons in that field at 1 K are better than 99% polarized. By doping a suitable solid target material with paramagnetic radicals to provide unpaired electron spins, one can make use of the highly polarized state of the electrons. The dipole-dipole interaction between the nucleon and the electron leads to hyperfine splitting, providing the coupling between the two spin species. By applying a suitable microwave signal, one can populate the desired spin states. The target spin direction will be reversed once every 8 hours by microwave frequency changes, while the magnet field is unchanged.

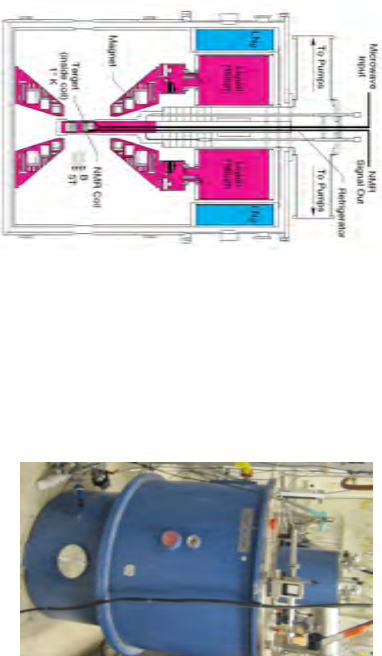


Figure 3. Schematic drawing of the polarized  $\text{NH}_3$  target (left) and existing magnet (right).

We will use frozen ammonia ( $\text{NH}_3$ ) as the target material and create the paramagnetic radicals (roughly  $10^{19}$  spins/ml) through irradiation with a high intensity electron beam at NIST. Our collaborators at UVA have agreed to build a new cryogenic refrigerator, which works on the principle of liquid  $^4\text{He}$  evaporation and can cool the bath down to  $\sim 1$  K, by pumping. The vapor down to  $< 0.18$  Torr. UVA scientists have built many polarized systems over the last two decades and are world experts on such DNP targets. In parallel, our team will design and build the new target cell, microwave system and Nuclear Magnetic Resonance (NMR) system used to measure the polarization. The microwave system is used to induce the spin flip transition. NMR coils, placed inside the target, can determine the proton polarization to an accuracy of  $\sim \pm 4\%$ . The maximum polarization achieved with such a target is better than 92% and the  $\text{NH}_3$  bead packing fraction is about 60%. In our estimate for the statistical precision, we have assumed an average polarization of 80%. The polarization dilution factor, which is the ratio of free polarized protons to the total number of nucleons, is 3/17 for  $\text{NH}_3$ , due to the presence of nitrogen. The  $\text{NH}_3$  beads need to be replaced approximately every 5 days, due to the beam induced radiation damage. This work will involve replacing the target stick with a new insert, cooling down the target and performing a thermal equilibrium measurement. From previous experience, we estimate that this will take about a shift to accomplish. Careful planning of these changes will reduce the impact on the beam time. Furthermore, we will be running with two active targets on one stick, thus reducing any additional loss of beam time.

### 3. Expected results

In Figure 4, we present the expected statistical precision of the single spin asymmetry that can be obtained in a one year run. We assume an integrated number of protons on target of  $2.7 \times 10^{18}$ . The assumptions on which these calculations are based are discussed in Appendix 1.

Approximately 110,000 reconstructed Drell-Yan pairs can be collected per year, after applying geometry cuts similar to that of E906. A strong sensitivity to the sign and magnitude of the Sivers asymmetry is demonstrated for non-zero values. The magnitude of the Sivers function can be determined to better than 4%. Also shown in Figure 4 is a theoretical estimation of the possible magnitude of the Drell-Yan Sivers asymmetry from a phenomenological fit by Anselmino et al [14] to the existing valence quark SIDIS data. We note that the error band on the sea quark Sivers function is not well constrained, since the fits are not very sensitive to the sea quark contribution. During this experiment, we expect to clearly answer the following questions:

- What is the sign of the Sivers asymmetry for sea quarks in DY?
- Does the sea quark orbital angular momentum contribute significantly to the proton spin?

The systematic uncertainties, not shown in Figure 4, are expected to be smaller than the statistical errors, for small measured asymmetries. The systematic errors are generally proportional to the size of the asymmetry. The absolute error will be  $\sim 1\%$  and the relative error will be at the 4% level. Major sources of systematic error include uncertainties in the polarization, which contributes to the relative uncertainty, and the relative luminosity, which contributes to the absolute uncertainty.

In addition to these Drell-Yan events, we also expect to collect  $\sim 1$  million  $J/\psi$  events. Since a substantial fraction of  $J/\psi$  production at this kinematics originates from quark-antiquark

annihilation rather than gluon-gluon fusion, the single-spin asymmetry from  $J/\psi$  events is likely to be sensitive to the sea quark Sivers distribution [15].

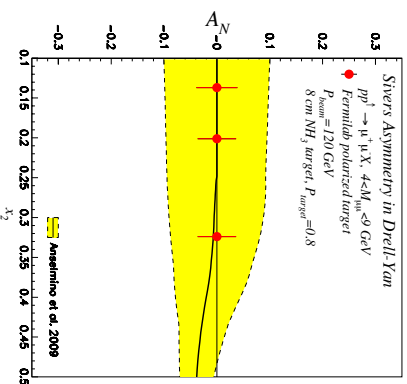


Figure 4. Estimated statistical precision for the DY Sivers asymmetry versus  $x_2$ . Also shown is the prediction from Anselmino [14] for the magnitude of the asymmetry. Note that we have extended the theoretical estimate below its valid minimum of  $x_2$  of 0.2, in order to guide the eye. There is currently no theoretical prediction available for the asymmetry below that value.

After a successful measurement with polarized  $\text{NH}_3$  is completed, a switch to polarized  $\text{ND}_3$  would allow us to examine the Sivers effect in the neutron versus the proton. This would provide separate Sivers functions for anti-up and anti-down quarks in the proton, similar to how E866 and E906 are performed. However, the expected  $\text{ND}_3$  polarization is only  $\sim 35\%$ , which results in reduced statistical precision for the same integrated luminosity.

Once a polarized proton beam is available for E1027, our polarized target will become a crucial component for performing double spin asymmetry measurements. This would allow us to develop a full spin physics program at Fermilab using the Drell-Yan process, since all of the required infrastructure will be available. For example, the Drell-Yan beam-target transverse double-spin asymmetry will provide direct access to the product of the valence and sea quark transverse spin distributions, without introducing the T-Odd spin-dependent quark fragmentation functions contained in the SIDIS measurements.

#### 4. Collaborators and required resources

For this LOI, the initial collaboration includes groups that have been heavily involved in previous Fermilab Drell-Yan measurements, as well as groups that successfully built and operated polarized  $\text{NH}_3$  targets. Many of the E906 collaborators will join this new experiment and continue to support and maintain the E906 spectrometer. LANL and UVA will develop and support the polarized target and existing superconducting magnet. In order to achieve transverse

polarization, the superconducting coils of the magnet have to be rotated. Oxford Instruments, the original manufacturer, will do this. To reach 1 K temperature in the refrigerator, large Roots pumps, provided by LANL, will pump on the refrigerator's He bath. Once the system is at 1 K, with the microwaves and beam as the only heat-loads (only  $\sim 1/4$  watt for beam), the system will evaporate roughly 100 liters of liquid He per day. This will necessitate a buffer receptacle for the exhaust helium. Liquid He will most likely be supplied from Dewars. We are studying the possibility of adding a He liquefier system. While such a system could be cost prohibitive for a two year run period, it would be preferable if this target would become part of the regular infrastructure of FNAL. In order to design and run such a liquefier plant, we would need support from FNAL. LANL will also provide the microwave system consisting of the Klystron, power supply and frequency meter, as well as the NMR system needed to determine the polarization in the target. The frozen ammonia beads will be irradiated by UVA and LANL personnel at NIST. They must be replaced after every 5 days of proton beam, requiring about one shift of access to the target.

The experiment may require beam-line improvements and new safety infrastructure from Fermilab, possibly including a pinhole collimator, final focusing quadrupole magnet set and an additional beam position monitor. These will reduce the probability of quenching the superconducting magnet. Preliminary discussions with the E906 beamline physicist (Mike Geelhoed) indicate that the existing upstream quadrupole may be adequate. A method for the safe venting of helium gas during a quench is required. A partial redesign of the target cave is required to accommodate the large Roots pumps, two He Dewars and liquid nitrogen supply. The EMAG and KEMAG magnet fields will require occasional reversals to minimize systematic errors. A convenient way to switch their polarities is necessary.

In Figure 5, we have assumed that liquid He would be supplied from two 1000 liter Dewars. We are currently studying two options for placing the Roots pumps, which are labeled as 1 and 2. In case 1, we would place the pump stand outside of the beam area on top of the shielding. For case 2, the stand would be in the cave. Shielding issues as well as pumping power will govern the final choice. Also drawn is the additional quadrupole for beam focusing. In addition, the overhead space will need to be increased, in order to allow for replacement of the target's  $\text{NH}_3$  beads every 5 days, due to the radiation damage. Depending on the location of the big Roots pumps, additional cave modifications may be needed in order to accommodate the pump's vacuum line to the magnet. Finally, the current crane in the cave has to be replaced with one with a higher lift capacity (2 ton) and lift rails installed that extend further upstream. This is necessary to perform any needed repairs to the magnet.

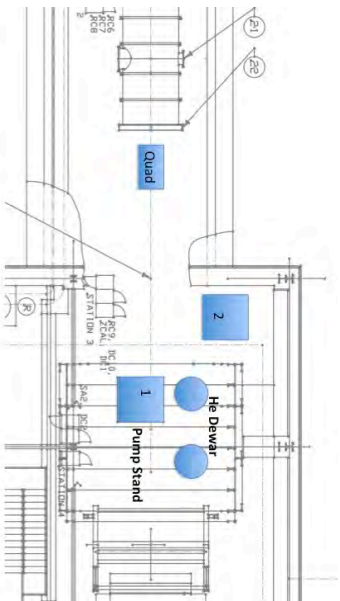


Figure 5. Top view of the E906 beam-line, target cave and proposed changes (in blue).

In Figure 6, we show a drawing of the target cave and shielding for E906, as viewed along the beam-line. The dashed blue line is the current cave ceiling, while the blue box represents the space needed for the polarized target. A minimum of 140" of vertical space is required above the floor, in order to accommodate the extraction of the target ladder. This would require raising the roof of the cave by roughly 32", through a partial restacking of the target cave shielding. This may, in turn, necessitate new MARS shielding calculations.

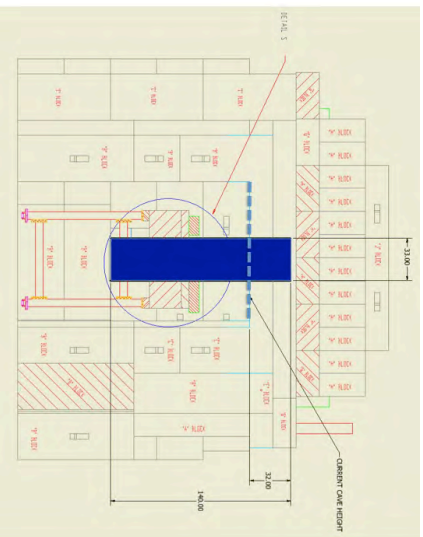


Figure 6. Beam's eye view of the E906 target cave, looking downstream toward the polarized target. The blue rectangle represents the height and vertical clearance required for the polarized target. The dashed line is the current (insufficient) cave height.

## Appendix 1. Rate estimates and expected precision

The Drell-Yan yields were calculated in a similar fashion to those for the E906 experiment, using the E906 GEANT 4 based Monte Carlo calculation for the acceptance. The Drell-Yan cross section was taken from PYTHIA using the CTTEQ5M parton distribution functions and verified against a modern NLO DY calculation from Vitiev, et al. The polarized target and a simplified holding magnetic field were added at the E906 target location. Effects due to fringe fields from the FMAAG have not yet been included, but will be carefully studied. A field clamp plate will be added to the FMAAG, to eliminate the  $\sim 15$  Gauss residual field measured in the target region that could degrade the polarization. We assume a target polarization of 80%, packing fraction (from the  $\text{NH}_3$  beads) of 60%, dilution factor of 3/17 and target length of 8 cm. The  $\text{NH}_3$  beads plus the surrounding He bath correspond to a total target areal density of  $\sim 5 \text{ g/cm}^2$ .

Approximately 110,000 DY events are expected for  $2.7 \times 10^8$  effective protons on target (one year), as shown in Table 1. This corresponds to  $1.0 \times 10^{13}$  protons per spill. The distribution of sampled parton momentum fraction, in terms of  $x_1$  and  $x_2$ , is shown in Figure 7. Good coverage for sea quarks in the target is obtained. Valence quarks are dominant in the beam. The integrated proton-nucleon luminosity, including 50% beam availability and 80% experimental livetime, is estimated to be  $6.5 \times 10^{42}$  per  $\text{cm}^2$ . The kinematic coverage is given in the table below. Since the spectrometer will be operating at very high rates, a good beam duty factor is essential to prevent high trigger rates and chamber occupancies. Poor duty factor hampered the first run of E906. Whatever solution is found for E906 should be adequate for our purpose.

- Kinematic range:  $4 < M < 8 \text{ GeV}$ ,  $0.2 < x_F < 0.8$

Cuts	Efficiency	Yield
All DY in the kinematic range	100%	$1.34\text{E}+08$
$\mu^+\mu^-$ accepted by all detectors	2%	$2.78\text{E}+06$
Accepted by trigger	50%	$1.39\text{E}+06$
$\mu^+\mu^-$ pair reconstructed (with target/dump separation cut)	8%	$1.11\text{E}+05$

Table 1. Drell-Yan yield estimates for a one-year long run.

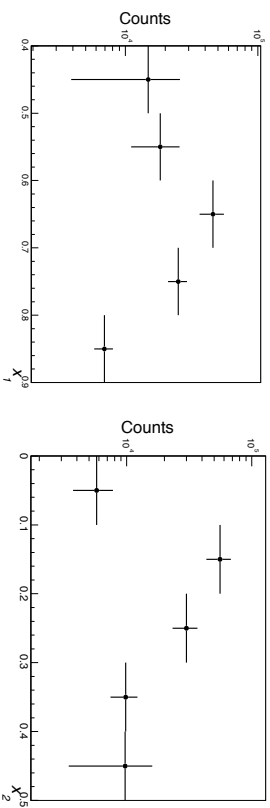


Figure 7. Expected distribution of Drell-Yan events, in terms of Bjorken- $x_1$  (beam) and  $x_2$  (polarized target). The vertical axis is number of events and error bars are statistical.

## References

1. D. Boer, M. Diehl, R. Milner, R. Venugopalan, W. Vogelsang, D. Kaplan, H. Montgomery and S. Vignor et al., “Glueons and the quark sea at high energies: Distributions, polarization, tomography”, arXiv:1108.1713 [nucl-th].
2. A. Accardi, J. L. Albacete, M. Anselmino, N. Armesto, E. C. Aschenauer, A. Bacchetta, D. Boer and W. Brooks et al., “Electron Ion Collider: The Next QCD Frontier - Understanding the glue that binds us all”, arXiv:1212.1701 [nucl-ex].
3. E. Aschenauer, A. Bazilevsky, K. Boyle, K. Eyser, R. Fatemi, C. Gagliardi, M. Grosse-Perdekamp, J. Lajoie and Z. B. Kang et al., “The RHIC Spin Program: Achievements and Future Opportunities”, arXiv:1304.0079 [nucl-ex].
4. D. Sivers, Phys. Rev. D41 (1990) 83.
5. D. L. Adams et al. [FNAL-E704 Collaboration], Phys. Lett. B 264, 462 (1991).
6. A. Airapetian et al. [HERMES Collaboration], Phys. Rev. Lett. 103, 152002 (2009).
7. M. Alekseev et al. [COMPASS Collaboration], Phys. Lett. B 673, 127 (2009).
8. X. Qian et al. [JLab Hall A Collaboration], Phys. Rev. Lett. 107:072003, 2011.
9. G. Garvey, Phys. Rev. C81 (2010) 055212 and E866 collaboration, Phys. Rev. Lett. 80 (1998) 3715-3718.
10. J. C. Collins, Phys. Lett. B536, 43–48 (2002).
11. Fermilab E1027 proposal, 2012.
12. S. Arnold, A. Metz, M. Schlegel, Phys. Rev. D79 (2009) 034005.
13. COMPASS-II collaboration, [http://www.compass.cern.ch/compass/proposal/compass-II\\_proposal/](http://www.compass.cern.ch/compass/proposal/compass-II_proposal/)
14. M. Anselmino, private communication, based on M. Anselmino et al. Eur. Phys. J. A39, 89–100 (2009).
15. M. Anselmino et al. Phys. Lett. B594 (2004) 97.

## E Quote For Liquefier



Quantum Technology Corp.

PMB 183, 250 H Street  
Blaine WA 98230 USA  
Tel: +1-604-222-5539, Fax: +1-604-677-5826  
Toll Free: +1-888-271-9466 Fax: +1-888-711-5222  
sales@quantum-technology.com



Quantum Technology Corp.

PMB 183, 250 H Street  
Blaine WA 98230 USA  
Tel: +1-604-222-5539, Fax: +1-604-677-5826  
Toll Free: +1-888-271-9466 Fax: +1-888-711-5222  
sales@quantum-technology.com

To: Mr. Andi Klein  
MS-H846, Group P-25  
LANL  
Los Alamos, NM 87545  
office: A138, Bldg 1, TAs3  
lab: 505 606 0662  
email: aklein@lanl.gov

Quotation #350703

Offer Los Alamos

July 5, 2015

Helium Liquefaction + Purification system

Table of Contents

- 1. Price
- 2. Delivery Schedule
- 3. Point of Delivery
- 4. Payments Terms
- 5. Sales and Use Taxes
- 6. Validity of the Quote
- 7. Appendices

<http://www.quantum-technology.com>

1. Price

Customer Liquefier refurbishment (estimation, pending on the actual state).....	\$30,000.00
RS Compression System for liquefier .....	\$149,000.00
Design of the whole system, valves and regulators (estimation).....	\$30,000.00
RDT between liquefier and dewar.....	\$12,000.00
Piping from liquefier to compressor.....	\$12,500.00
Purifier for the entire flow.....	\$65,000.00
<i>Option for Purifier: Automation (for purifier, see Appendix 1) .....</i>	<i>\$65,000.00</i>
High pressure helium recovery compressor.....	\$27,500.00
Gas Bag including control for recovery compressor and relief valve.....	\$11,500.00
Commissioning (price/day on site, expenses extra).....	\$1,500.00
Set of spare parts for purifier.....	\$3,000.00
Set of spare parts for HP compressor.....	\$1,800.00

Warranty: 1 year parts and factory service

Note: Performance Test and Manual are included

2. Delivery Schedule

Expected delivery date is 36 weeks from date of the PO.

<http://www.quantum-technology.com>



Quantum Technology Corp.

PMB 183, 250 H Street  
Blaine WA 98230 USA  
Tel: +1-604-222-5539, Fax: +1-604-677-5826  
Toll Free: +1-888-271-9466 Fax: +1-888-711-5222  
sales@quantum-technology.com

### 3. Point of delivery

Above prices are valid for point of fabrication, Vancouver, Canada.

### 4. Payment Terms

- 30% of the contract value at the time of receiving the Purchase Order
- 50% of the contract value at the beginning of the system fabrication
- 15% of the contract value after issuance of "Notice of Completion"
- 5% of the contract value after submission of the final documentation

### 5. Sales and Use Taxes

Above prices include value added, sales and/or use taxes in North America, all customs, local taxes at the customer site are the obligation of the customer.

### 6. Validity of the Quote

This quotation is valid for sixty (60) days.

<http://www.quantum-technology.com>



Quantum Technology Corp.

PMB 183, 250 H Street  
Blaine WA 98230 USA  
Tel: +1-604-222-5539, Fax: +1-604-677-5826  
Toll Free: +1-888-271-9466 Fax: +1-888-711-5222  
sales@quantum-technology.com

### Appendix 1. Purifier characteristics

QUANTUMPURE Q016.5-200 Operating Parameters:

Inlet purity: Can be 98%, 99% or 99.5%

The inlet purity will affect the quantity of gas which can be purified before regeneration.

Outlet purity >99.999%

Throughput of liquefier (guaranteed) is 50 liquid litres per hour of liquid helium.

Monitoring:

Continuous monitoring and digital display of helium purity to prevent low purity gas from going out.

Cooling: Requires LN2 from bulk tank at 2-3 bar absolute

Cooldown time: Requires 1 hour cooldown prior to use

Operational time: Depends on inlet purity. For an inlet purity of 99.5% can purify 1000 L of liquid helium equivalent prior to regeneration

Regeneration cycle: Overnight warmup and venting of impurities

**Automation (offered as an option):**

A PLC control system automatically controls the following features:

- Automatic liquid nitrogen filling of the QUANTUMPURE
- Automatic display of helium purity with digital display
- Automatic closing of outlet valve before helium purity falls below 99.995%
- Automatic cooldown of system preparing for purification

**Manual process:**

Regeneration is manual after an overnight warmup.

**Operating modes:**

Purifying of helium gas from new gas bottles to the system

Purifying of recovered helium gas to the system (recovery system not included in this item)

**Infrastructure required:**

Electric power as per customer request

Room temperature: 10-30C

Compressed air: 6-10 bar (0.1 cubic meter/hour) for instruments

Cooling water: not required

One bottle of helium 6.0 reference gas (for purity meter calibration).

Liquid nitrogen: 2-3 bar a (~0.6 liter of liquid nitrogen per liter of liquid helium)

<http://www.quantum-technology.com>

PMB 183, 250 H Street  
Blaine WA 98230 USA  
Tel: +1-604-222-5539, Fax: +1-604-677-5826  
Toll Free: +1-888-271-9466 Fax: +1-888-711-5222  
sales@quantum-technology.com

(from bulk tank)

**Includes:**  
Interconnecting piping, valves and controls.  
Engineering design of system  
Floor plan layout.

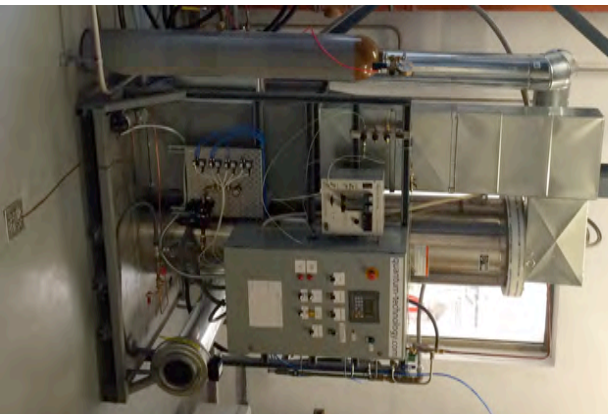


Figure 1. Photo of a recent recovery and purification project in Europe for a 50 liter/hr turbine liquefier system. PLC in Figure is optional in this quotation.

<http://www.quantum-technology.com>

PMB 183, 250 H Street  
Blaine WA 98230 USA  
Tel: +1-604-222-5539, Fax: +1-604-677-5826  
Toll Free: +1-888-271-9466 Fax: +1-888-711-5222  
sales@quantum-technology.com

## Appendix 2. RS Compressor Module

The RS Compressor Assembly is a skid-mounted, rotary screw compressor which has proven to have exceptional long-term reliability with low maintenance.

The compressor is a vertical assembly consisting of an encapsulated oil-flooded helical screw assembly, a drive motor, and an oil separation/impingement plate. The oil provides lubrication, sealing of the compressor rotors and compressor cooling. Adequate cooling is provided to prevent oil breakdown due to high temperature.

The oil removal system consists of the oil separation/impingement plate located within the compressor pump housing followed by coalescing filters connected in series wherein oil is separated from the gas stream and returned to the oil reservoir in the compressor sump. Following the last coalescer, the compressed helium gas flows through a charcoal bed adsorber where any traces of oil vapor are removed.

The oil cooler consists of a water-to-oil heat exchanger and the gas aftercooler is a water-to-gas heat exchanger. The standard motor starter supplied with the compressor skid is a reduced in-rush current motor starter that is wall mounted at site by the customer. The compatible hermetic motor and motor starter can be supplied to operate on most common voltages at either 50 or 60 Hertz.

RS Compressor shown below.



The compressor is hermetic with a compressor drive motor located on the discharge side of the pump. The shaft seal required for externally driven compressors has been eliminated. Therefore, it is possible to operate on sub-atmospheric suction without the danger of air contamination as long as the interconnecting piping between compressor suction and liquefier assembly is maintained leak tight.

The screw compressor includes a hydraulically operated slide valve which loads the compressor via button on the OTF panel on the liquefier. The slide valve loading changes the displacement of the pump from approximately 65 % flow to 100 % flow and is manually positioned by the operator at start-up. To

<http://www.quantum-technology.com>

# Quantum

Quantum Technology Corp.

PMB 183, 250 H Street  
Blaine WA 98230 USA  
Tel: +1-604-222-5539, Fax: +1-604-677-5826  
Toll Free: +1-888-271-9466 Fax: +1-888-711-5222  
sales@quantum-technology.com

provide for reduced capacity during periods of low liquefaction capacity demand, the operator can run the compressor in unload position. The slide valve location changes the mass flow of the system. In the unload position, the input power is reduced, thus providing for economical operation during periods of low demand. The slide valve will automatically unload at shutdown of the compressor.

Instrumentation includes suction and discharge pressure gauges and an elapsed time meter. Compressor is operated from the local push buttons for start/stop and slide- valve loading are provided. In addition, these features can be modulated from the Helium Liquefier control panel.

Safety switches are provided for limiting discharge pressure and temperature, low suction pressure, motor winding temperature, and low oil pressure. A first fault annunciator is provided (in OIT) to indicate the cause of any shutdown.

Compressor provides pure helium supply and/or storage up to 18 bar pressure. The compressor can be operated with a suction pressure as low as 0.5 bar and as high as 2 bar with a discharge pressure as high as 18 bar, resulting in a helium mass flow rate of 18 g/s using a 60 Hz power source (15 g/s using 50 Hz power).

Power Consumption: 95 kW, 460 V, 3 Phase, 60 Hertz (80 kW, 50 Hz) Water Cooling Requirements: 57 l/minute (15 gal/min.) @ 24 C & 310 kPa (45 psig) Weight: 1,135 kg (2,500 lbs) Dimensions: 1,450 x 1,350 x 1,480 mm (57 x 53 x 58 in)

#### Utility requirements compressor

Power: Each Model RS Compressor requires approximately 95 kW, 460 V, 3Ø, 60 Hz or 80 kW, 50 Hz power when operating fully loaded. Actual power consumption will vary depending on the mass flow rate required for each application. Voltage should be specified with all orders.

Water: 57 liters/minute (15 GPM) at 24°C (75°F) and 310 kPa (45 psig) supply pressure. Weight: 1,135 kg (2,500 lbs) Dimensions: 1,450 x 1,350 x 1,480 mm (57 x 53 x 58 in).

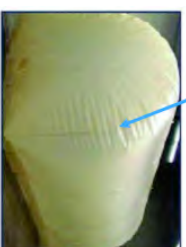
<http://www.quantum-technology.com>

# Quantum

Quantum Technology Corp.

PMB 183, 250 H Street  
Blaine WA 98230 USA  
Tel: +1-604-222-5539, Fax: +1-604-677-5826  
Toll Free: +1-888-271-9466 Fax: +1-888-711-5222  
sales@quantum-technology.com

EXAMPLE OF INSTALLATION OF THE LIQUEFACTION-PURIFICATION SYSTEM at CALTECH, USA



1. Gas bag
2. 100kWatt Liquefier (47 litres/hour)
3. Liquid storage dewar (1000 litres)
4. Purifier – LN<sub>2</sub> cooled

<http://www.quantum-technology.com>

PMB 183, 250 H Street  
Blaine WA 98230 USA  
Tel: +1-604-222-5539, Fax: +1-604-677-5826  
Toll Free: +1-888-271-9466 Fax: +1-888-711-5222  
sales@quantum-technology.com

### Appendix 3. High Pressure Helium Recovery Compressor

#### Characteristics:

Pressure: 4500 psi  
Flow rate: 7.0 cfm  
Motor size: 7.5 HP  
Filtering system included  
Electric powered: 3 phase, per user requirements



#### Standard Scope of Supply

- Multi-stage, aircooled piston compressor.
- Electric motor drive.
- Automatic start-stop control.
- Emergency stop pushbutton.
- Automatic condensate drain system with condensate collector.
- PLC-based control system (UL).
- Full-voltage motor starter.
- Operator keypad for start, stop, reset.
- Backlit LCD display.

<http://www.quantum-technology.com>

PMB 183, 250 H Street  
Blaine WA 98230 USA  
Tel: +1-604-222-5539, Fax: +1-604-677-5826  
Toll Free: +1-888-271-9466 Fax: +1-888-711-5222  
sales@quantum-technology.com

- Low/High inlet pressure switch with gauge.
- High temperature switch.
- Final pressure switch.
- Hourmeter.
- Coalescing separator at outlet.
- Sound attenuated enclosure.

<http://www.quantum-technology.com>

## References

- [1] J. Ashman et al., Nucl. Phys. B 328,1 (1989)
- [2] D. Boer, M. Diehl, R. Milner, R. Venugopalan, W. Vogelsang, D. Kaplan, H. Montgomery and S. Vigdor et al., "Gluons and the quark sea at high energies: Distributions, polarization, tomography", arXiv:1108.1713 [nucl-th]
- [3] A. Accardi, J. L. Albacete, M. Anselmino, N. Armesto, E. C. Aschenauer, A. Bacchetta, D. Boer and W. Brooks et al., Electron Ion Collider: The Next QCD Frontier - Understanding the glue that binds us all?, arXiv:1212.1701 [nucl-ex].
- [4] E. Aschenauer, et al., The RHIC Spin Program: Achievements and Future Opportunities, arXiv:1304.0079 [nucl-ex]
- [5] A. Airapetian Phys Rev. **D64** (2001) 097101
- [6] D. L. Adams Phys. Lett. **B 264** (1991), 462
- [7] D. Sivers, Phys. Rev. **D41** (1990) 83
- [8] D. Boer and P. J. Mulders Phys. Rev. **D 57**, (1998) 5780
- [9] J. Huang, Z. B. Kang, I. Vitev and H. Xing, Phys. Rev. **D 93**,(2016) 014036
- [10] E. A. Hawker et al., Phys. Rev. Lett. **80** (1998) 3715
- [11] D. L. Adams et al. [FNAL-E704 Collaboration], Phys. Lett. **B264** (1991) 462
- [12] A. Airapetian et al. [HERMES Collaboration], Phys. Rev. Lett. **103** (2009) 152002
- [13] M. Alekseev et al. [COMPASS Collaboration], Phys. Lett. **B673** (2009) 127
- [14] X. Qian et al. [JLab Hall A Collaboration], Phys.Rev.Lett. **107** 2011 072003
- [15] H. Gao, et al. E12-11-108 proposal, 2012 [https://www.jlab.org/exp\\_prog/proposals/11/PR12-11-108.pdf](https://www.jlab.org/exp_prog/proposals/11/PR12-11-108.pdf)
- [16] Long Range Plan for Nuclear Science [http://science.energy.gov/media/np/nsac/pdf/2015LRP/2015\\_LRPNS\\_091815.pdf](http://science.energy.gov/media/np/nsac/pdf/2015LRP/2015_LRPNS_091815.pdf)
- [17] G. Garvey, Phys. Rev. **C81** (2010) 055212 and E866 collaboration, Phys. Rev. Lett. **80** (1998) 3715
- [18] J. C. Collins, Phys. Lett. **B536** (2002) 43
- [19] Fermilab E1027 proposal, 2012 <http://ccd.fnal.gov/techpubs/fermilab-reports-proposal.html> (FERMILAB-PROPOSAL-1027)
- [20] SD . Drell and TM. Yan, Phys. Rev. Lett. **25** (1971) 316
- [21] TMD Collaboration for the Coordinated Theoretical Approach to Transverse Momentum Dependent Hadron Structure in QCD, J.W. Qiu, W. Detmold, *et al.*, 2015
- [18] J. C. Collins, Nucl. Phys. B **396**, 161 (1993)

- [22] A. V. Belitsky, X. J and F. Yuan, Nucl. Phys. B 656 (2003) 165
- [23] D. Boer, P. J. Mulders and F. Pijlman, Nucl. Phys. B **667**, 201 (2003)
- [24] P. J. Mulders, PoS QCDEV **2015**, 005 (2015) [arXiv:1510.05871 [hep-ph]]
- [25] M. G. Echevarria, A. Idilbi, Z. B. Kang and I. Vitev, Phys. Rev. D **89**, 074013 (2014)
- [26] S. M. Aybat, J. C. Collins, J. W. Qiu and T. C. Rogers, Phys. Rev. D **85**, 034043 (2012)
- [27] S. M. Aybat and T. C. Rogers, Phys. Rev. D **83**, 114042 (2011)
- [28] P. Sun and F. Yuan, Phys. Rev. D **88**, 114012 (2013)
- [29] Collins, John C. and Soper, Davison E., Nucl. Phys. B **193**, 391 (1981)
- [30] S. Arnold, A. Metz, M. Schlegel, Phys. Rev. **D79** (2008) 034005
- [31] Ji, Xiang-dong and Ma, Jian-ping and Yuan, Feng, Phys. Rev. D **71**, 034005 (2005)
- [32] Collins, John, Foundations of Perturbative QCD, Cambridge, UK: Univ. Pr. (2011)
- [33] Becher, Thomas and Neubert, Matthias, Eur. Phys. J. C **71**, 1665 (2011)
- [34] Echevarria, Miguel G. and Idilbi, Ahmad and Scimemi, Ignazio, JHEP **1207**, 002 (2012)
- [35] Chiu, Jui-Yu and Jain, Ambar and Neill, Duff and Rothstein, Ira Z., JHEP **1205**, 084 (2012)
- [36] Ji, Xiangdong and Sun, Peng and Xiong, Xiaonu and Yuan, Feng, Phys. Rev. D **91**, 074009 (2015)
- [37] Jaffe, R, “Where does the proton really get its spin?”, Physics Today. 48 (9): 24-30, (1995)
- [38] D. de Florian, R. Sassot, M. Stratmann and W. Vogelsang, Phys. Rev. Lett. **113**, 012001 (2014)
- [39] S. Meissner, A. Metz and K. Goeke, Phys. Rev. D **76**, 034002 (2007)
- [40] A. Bacchetta and M. Radici, Phys. Rev. Lett. **107**, 212001 (2011)
- [41] B. U. Musch, P. Hagler, M. Engelhardt, J. W. Negele and A. Schafer, Phys. Rev. D **85**, 094510 (2012)
- [42] L. Adamczyk *et al.* [STAR Collaboration], Phys. Rev. Lett. **116**, 132301 (2016)
- [43] M. Anselmino, M. Boglione, U. D’Alesio, S. Melis, F. Murgia and A. Prokudin, Phys. Rev. D **79**, 054010 (2009)
- [44] Aidala, C.A. and Field, B. and Gamberg, L.P. and Rogers, T.C., Phys. Rev. D **89**, 094002 (2014)
- [45] Kang, Zhong-Bo and Xiao, Bo-Wen and Yuan, Feng, Phys. Rev. Lett. **107**, 152002 (2011)
- [46] Leader, Elliot and Lorcé, Cédric, Phys. Rept. **541**, 163-248 (2014)

- [47] Ji, Xiang-Dong, Phys. Rev. Lett. **78**, 610-613 (1997)
- [48] K. F. Liu *et al.*, PoS LATTICE **2011**, 164 (2011)
- [49] L, Adamczyk *et al.*, Phys. Rev. Lett. **116**, 132301 (2016)
- [50] E906 collaboration, NIM article in preparation
- [51] G. R. Court, *et al.*, NIM **A 324** (1993) 433
- [52] D, Crabb, NIM in Phys. Res. **A356** (1995) 9
- [53] D. Keller, NIM **A 728** (2013) 133-144
- [54] O. Kahn, Molecular Magnetism; VCH: New York, (1993)
- [55] G. R. Court *et al* NIM in Phys. Res.,**A527** (2004) 253
- [56] Kadansky V. “Photoproduktion negativer Pionen an einem polarisierten Neutronentarget”, PhD. thesis. University of Bonn. BONN-IR-75-54 (1975)
- [57] C. Dulya *et al.* NIM **A398** (1997) 109
- [58] K. B. Unser, AIP Conf. Proc. 252, 266 (1992)
- [59] M. Anselmino private communication, based on M. Anselmino *et al.* Eur. Phys. J. **A39** (2009) 89
- [60] O. E. Krivosheev and N. V. Mokhov, A new MARS and its applications’, Fermilab-Conf-98/043 (1998) and SARE3 KEK Proceedings 97-5 (1997)
- [61] G. R. Court , *et al.* Nucl. Instr. & Meth. **A324** (1993) 433
- [62] <http://pac.fnal.gov/meetings/> Recommendations 2013
- [63] <http://pac.fnal.gov/meetings/> Recommendations 2015
- [64] A. Airapetian, Phys Rev. Lett. **103** (2009) 152002
- [65] F. Yuan, Phys. Rev. D **78**, 014024 (2008)
- [66] Z.-B. Kang, Private communications. (2016)